CANCER

The IDH-TAU-EGFR triad defines the neovascular landscape of diffuse gliomas

Ricardo Gargini[1,2]*, Berta Segura-Collar[2]*, Beatriz Herránz[2,3], Vega García-Escudero[1,4], Andrés Romero-Bravo[2], Felipe J. Núñez[5], Daniel García-Pérez[6], Jacqueline Gutiérrez-Guamán[7], Angel Ayuso-Sacido[8,9,10], Joan Seoane[11,12,13], Angel Pérez-Núñez[6], Juan M. Sepúlveda-Sánchez[7], Aurelio Hernández-Laín[7], María G. Castro[5], Ramón García-Escudero[7,12,14], Jesús Ávila[1,15†], Pilar Sánchez-Gómez[2†]

Gliomas that express the mutated isoforms of isocitrate dehydrogenase 1/2 (IDH1/2) have better prognosis than wild-type (wt) IDH1/2 gliomas. However, how these mutant (mut) proteins affect the tumor microenvironment is still a pending question. Here, we describe that the transcription of microtubule-associated protein TAU (*MAPT*), a gene that has been classically associated with neurodegenerative diseases, is epigenetically controlled by the balance between wt and mut IDH1/2 in mouse and human gliomas. In IDH1/2 mut tumors, we found high expression of TAU that decreased with tumor progression. Furthermore, *MAPT* was almost absent from tumors with epidermal growth factor receptor (*EGFR*) mutations, whereas its trancription negatively correlated with overall survival in gliomas carrying wt or amplified (amp) *EGFR*. We demonstrated that the overexpression of TAU, through the stabilization of microtubules, impaired the mesenchymal/pericyte-like transformation of glioma cells by blocking EGFR, nuclear factor kappa-light-chain-enhancer of activated B (NF-κB) and the transcriptional coactivator with PDZ-binding motif (TAZ). Our data also showed that mut EGFR induced a constitutive activation of this pathway, which was no longer sensitive to TAU. By inhibiting the transdifferentiation capacity of EGFRamp/wt tumor cells, TAU protein inhibited angiogenesis and favored vascular normalization, decreasing glioma aggressiveness and increasing their sensitivity to chemotherapy.

INTRODUCTION

Diffuse gliomas are classified and graded according to histological criteria. They include low- and intermediate-grade gliomas [herein called lower-grade gliomas (LGGs)], which encompass World Health Organization (WHO) grades 2 and 3, and the highly aggressive WHO grade 4 glioblastomas (GBMs), characterized by 5-year survival rates of 5%. They are categorized on the basis of the increments in cellular atypia and mitotic activity. Moreover, GBMs are characterized by the specific presence of areas of necrosis and robust neoangiogenesis and are considered one of the most vascularized cancers. LGGs have a better prognosis, although many of these tumors progress into secondary GBMs, albeit at highly variable intervals, with survival rates that go from 1 to 15 years (*1*). Unfortunately, little is known about the factors that drive this transition from LGG to GBM.

A substantial effort has been made in the last two decades to characterize the genetic modifications associated with gliomas. Some of them have been incorporated into the novel WHO classification. Particularly, the analysis of mutations in the isocitrate dehydrogenase 1/2 (*IDH1/2*) genes, which are associated with a more favorable prognosis in gliomas (*2*), is now common in clinical practice. IDH1/2 mutated proteins induce the accumulation of the oncometabolite, 2-hydroxyglutarate (2-HG), which competes with the α-ketoglutarate (α-KG) produced by the wild-type (wt) IDH enzymes and blocks ten-eleven translocation (TET)–mediated DNA demethylation. This process generates a CpG island methylator phenotype (G-CIMP), which is associated with a general suppression of gene expression (*3*). Moreover, 2-HG inhibits histone demethylases, which further contribute to this phenotype (*4*). By contrast, wt IDH1 promotes the metabolic adaptation of GBM cells to support aggressive growth (*5*). Therefore, it has been proposed that the balance between wt and mutant (mut) IDH1/2 function determines the clinical outcome of gliomas, including their sensitivity to radiation and chemotherapy (*6*).

Within the new subclasses of high-grade gliomas [proneural (PN), classic (CL), or mesenchymal (MES)], *IDH1/2* mutations are accumulated in the first group, which is enriched in secondary GBMs and includes tumors with a better clinical prognosis (*7*). By contrast, mutations in epidermal growth factor receptor (*EGFR*) accumulate in the CL and MES subtypes. This gene is mutated and/or amplified (amp) in a large percentage of diffuse gliomas, and it has been associated with proliferation and survival, as well as with the invasive properties of glioma cells (*7*, *8*).

Several cytoskeletal proteins have been involved in tumor progression. TAU, encoded by the gene microtubule-associated protein TAU (*MAPT*), is well known for its relevance in Alzheimer's disease (AD), although it is also expressed in healthy brains, where it controls

[1]Centro de Biología Molecular "Severo Ochoa" (CSIC-UAM), Madrid 28049, Spain. [2]Neurooncology Unit, Instituto de Salud Carlos III-UFIEC, Madrid 28220, Spain. [3]Facultad de Medicina de la Universidad Francisco de Vitoria, Madrid 28223, Spain. [4]Dto. de Anatomía, Histología y Neurociencia, Facultad de Medicina de la Universidad Autónoma, Madrid 28029, Spain. [5]Department of Neurosurgery/Department of Cell & Developmental Biology, University of Michigan School of Medicine, Ann Arbor, MI 48109, USA. [6]Dto. Neurocirugía, Hospital 12 de Octubre, Univ. Complutense, Madrid 28041, Spain. [7]Instituto de Investigaciones Biomédicas I+12, Hosp. 12 de Octubre, Madrid 28041, Spain. [8]Fundación de Investigación HM Hospitales, HM Hospitales, Madrid 28015, Spain. [9]Facultad de Medicina (IMMA), Universidad San Pablo-CEU, Madrid 28925, Spain. [10]IMDEA Nanoscience, Madrid 28049, Spain. [11]Vall d'Hebron Institute of Oncology (VHIO), Barcelona 08035, Spain. [12]Centro de Investigación Biomédica en Red de Cáncer (CIBERONC), ISCIII, Madrid 28029, Spain. [13]Institució Catalana de Recerca i Estudis Avançats (ICREA), Barcelona 08010, Spain. [14]Unidad de Oncología Molecular, CIEMAT, Madrid 28040, Spain. [15]Centro de Investigación Biomédica en Red sobre Enfermedades Neurodegenerativas (CIBERNED), ISCIII, Madrid 28029, Spain.
*These authors contributed equally to this work.
†Corresponding author. Email: psanchez@isciii.es (P.S.-G.); jesus.avila@csic.es (J.A.)

neural development and synaptic transmission (*9*). In addition, TAU and other microtubule-stabilizing agents like taxanes modulate protein and organelle trafficking (*10*, *11*), which could be relevant for cancer cells. A possible comorbidity of dementias and GBMs had been suggested (*12*), which led us to perform a bioinformatic analysis of brain gene expression. We found that *MAPT*, among other genes related to neurodegeneration, is expressed in gliomas, where it seems to correlate negatively with tumor progression (*13*). On the basis of these data, we decided to conduct a more comprehensive characterization of TAU in this deadly pathology. Here, we found that the expression of this protein depends on the genetic status of *IDH1/2*, being enriched in LGG and PN gliomas, where it hinders tumor progression. Mechanistically, TAU inhibited the EGFR–nuclear factor κB (NF-κB)–TAZ (WWTR1, WW Domain Containing Transcription Regulator 1) signaling pathway, provided that no EGFR mutations were present. By blocking this cascade, TAU impeded the capacity of the tumor cells to transdifferentiate into MES/pericyte-like cells, which participate in the processes of angiogenesis and neovascularization. As a consequence, TAU favored the normalization of the glioma's vasculature and hampered tumor progression.

RESULTS

High expression of MAPT correlates inversely with glioma aggressiveness

To validate our previous results (*13*), we performed a thorough analysis of the expression of *MAPT* in gliomas. The in silico study of the glioma dataset from The Cancer Genome Atlas (TCGA) showed that, as expected, the transcription of *MAPT* decreased as the tumor grade increased, at least in astrocytomas (Fig. 1A and fig. S1A and B). Moreover, a higher transcription of this gene was associated with an increased overall survival of patients with glioma (Fig. 1, B and C, and fig. S1, C to F). These results prompted us to perform an immunohistochemical (IHC) staining on glioma samples, which showed that TAU protein was clearly expressed in the cytoplasm of tumor cells, with a very different pattern to the one observed in normal tissue (NT) (Fig. 1D and fig. S1G). Besides, we found a high amount of TAU in a subset of the gliomas analyzed by Western blot (WB) (Fig. 1E). The quantification of the IHC staining (Fig. 1F) and the WB (Fig. 1G) confirmed that TAU was enriched in LGGs compared with GBMs. Although this accumulation could explain by itself the survival data, we found that the transcription of *MAPT* correlated with an increased overall survival in independent GBM (Fig. 2A) and LGG (Fig. 2B) cohorts. Similar results were obtained when we measured *MAPT* by quantitative reverse transcription polymerase chain reaction (qRT-PCR) analysis in our own GBM cohort (Fig. 2C). Collectively, these results support the idea that this gene is associated with a less aggressive behavior of gliomas, independently of the tumor grade. Furthermore, we found a marked decrease in the expression of *MAPT* in disease-free versus progressed tumors (Fig. 2D). To confirm these observations, we performed a longitudinal IHC quantification of TAU in primary LGGs and their recurrent paired samples. We found a consistent reduction in TAU in those tumors that had progress into a more aggressive phenotype (Fig. 2E), which was not observed when there was no change in the histological classification of the recidives (Fig. 2F). These results suggest that TAU down-regulation might be important for the tumors to relapse after surgical resection, which is a critical step in the mortality related to this pathology.

To further asses the presence of TAU in glioma cells and its participation in tumor aggressiveness, we analyzed its expression in a panel of patient-derived xenografts (PDXs), grown subcutaneously and devoided of any trapped neurons. As we had previously observed in tumor samples (Fig. 1E), the quantity of the TAU protein in the PDXs was highly variable (Fig. 2G and fig. S2A). It is important to remark that in the TAU-high tumors, a substantial percentage of glial fibrillary acidic protein (GFAP) cells were positive for TAU staining (fig. S2, A and B), further supporting the specific presence of this protein in glioma cells.

To investigate whether the amount of TAU could affect tumor behavior, we injected some of the patient-derived tumor cells into the brains of immunodeficient mice, and we observed that the TAU-high cells grew much slower than the TAU-low cells (Fig. 2H). The differences in *MAPT* expression in the tumors were validated by qRT-PCR, using human-specific primers (Fig. 2I). Moreover, the overexpression of this gene in a TAU-deficient glioma cell line (12o15) delayed tumor formation (Fig. 2J and fig. S2C), whereas its down-regulation in TAU-enriched cells (12o02) increased their aggressive behavior (Fig. 2K and fig. S2D). Together, our results confirmed the presence of TAU in the tumor cells of several gliomas, especially in the less aggressive ones. In addition, they suggest that this protein could be playing an active role in tumor progression.

The expression of MAPT in gliomas is regulated by IDH function

To investigate the regulation of *MAPT* expression in gliomas, we analyzed the genetic background of these tumors in relation to the quantity of its mRNA, and we found that *IDH1* mutations accumulate in *MAPT*-high gliomas (Fig. 3A). This correlation was validated using a volcano plot analysis (Fig. 3B). Furthermore, TAU protein was detected in most of the tumor cells that express the most common IDH1 mutation (R132H) (fig. S3, A and B), further confirming that the protein is expressed in tumor cells. We then measured TAU IHC staining in wt and mut *IDH* gliomas, and we found a clear enrichment of high- and medium-stained sections in the second group (Fig. 3C). These results highlight the correlation between the presence of IDH mutations and the expression of TAU, which seems to be independent of the tumor grade as we found a higher amount of *MAPT* transcription in *IDH* mut compared with *IDH* wt tumors in the GBM (fig. S3C) and in the LGG (fig. S3D) TCGA cohorts. To confirm this relationship, we analyzed a recently published glioma model, in which IDH1 wt or IDH R132H has been expressed in an *ATRX* mut background (*14*). As expected, there was a delay in the tumor growth in the presence of mut IDH1 (Fig. 3D). Moreover, we measured an increase in the quantity of TAU in the mut compared with the wt dissected allografts (Fig. 3E), suggesting that the expression of TAU in gliomas might be induced by mut IDH proteins.

The G-CIMP phenotype, which is associated with the presence of *IDH* mutations, is supposed to block the transcription of many genes (*3*). However, it also activates certain others, especially those involved in the tumorigenesis of LGG [like the platelet-derived growth factor receptor alpha (*PDGFRA*) oncogene] through the disruption of the repressive structure of the CCCTC-binding factor (CTCF) insulator protein (*15*). We observed an increased expression of *MAPT* in the G-CIMP GBM subtype (fig. S4A), as well as a strong correlation between the transcription of *MAPT* and *PDGFRA* in the TCGA samples (fig. S4B). To test whether *MAPT* expression could be epigenetically controlled by IDH mutations, we first analyzed the presence of CpG islands in its promoter region by using the Xena

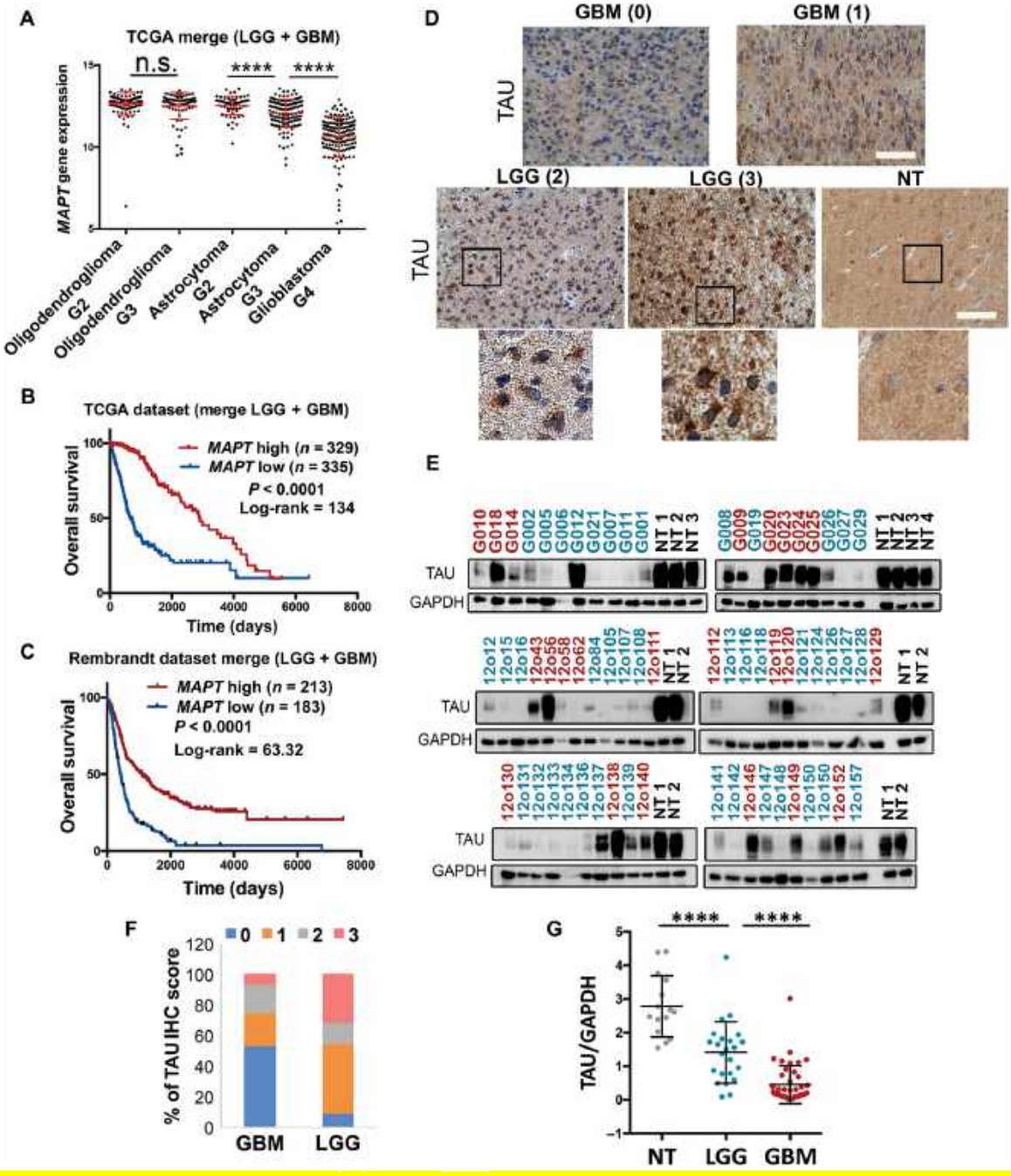

Fig. 1. TAU is expressed in gliomas and is enriched in LGG. (**A**) Analysis of *MAPT* expression by RNA sequencing (RNA-seq) in gliomas (TCGA cohort), grouped according to the WHO classification ($n = 692$). (**B** and **C**) Kaplan-Meier overall survival curves of patients from the TCGA (LGG + GBM) ($n = 664$) and the Rembrandt (LGG + GBM) ($n = 396$) cohorts. Patients in each cohort were stratified into two groups based on high and low *MAPT* expression values; log-rank (Mantel-Cox) test. (**D**) Representative pictures of the TAU IHC staining in gliomas and normal tissue (NT). The TAU IHC score is represented in parentheses, and an amplified section of the last three images is shown on the bottom. (**E**) WB analysis of TAU in tumor tissue extracts from patients diagnosed with LGG (red) and GBM (blue). NT was used as a control of TAU expression and glyceraldehyde-3-phosphate dehydrogenase (GAPDH) as a loading control. (**F**) Percentage of tumors [GBM ($n = 55$) and LGG ($n = 22$)] with different TAU IHC score. (**G**) Quantification of the relative amount of TAU in the WB in (E). Data are shown as means ± SD; Student's *t* test; ****$P \leq 0.0001$. n.s., not significant. Scale bars, 50 μm.

genome browser. We identified three of them in the 5′ region of the transcription initiation site (fig. S4C), which correlate with the sites previously described (*16*). Using epigenetic data from the TCGA dataset (LGG cohort), we compared the methylation of the whole promoter region in mut versus wt IDH tumors. We observed an increased methylation in CpG:26 (Fig. 3F and fig. S4, D and E) and in some parts of CpG:302 (fig. S4, D and E) in the mut tumors. However, when we analyzed the chromatin immunoprecipitation–sequencing (ChIP-seq) data of the CTCF binding to the different clusters, we observed that only the binding to the CpG:26 site was lost in the *IDH mut*

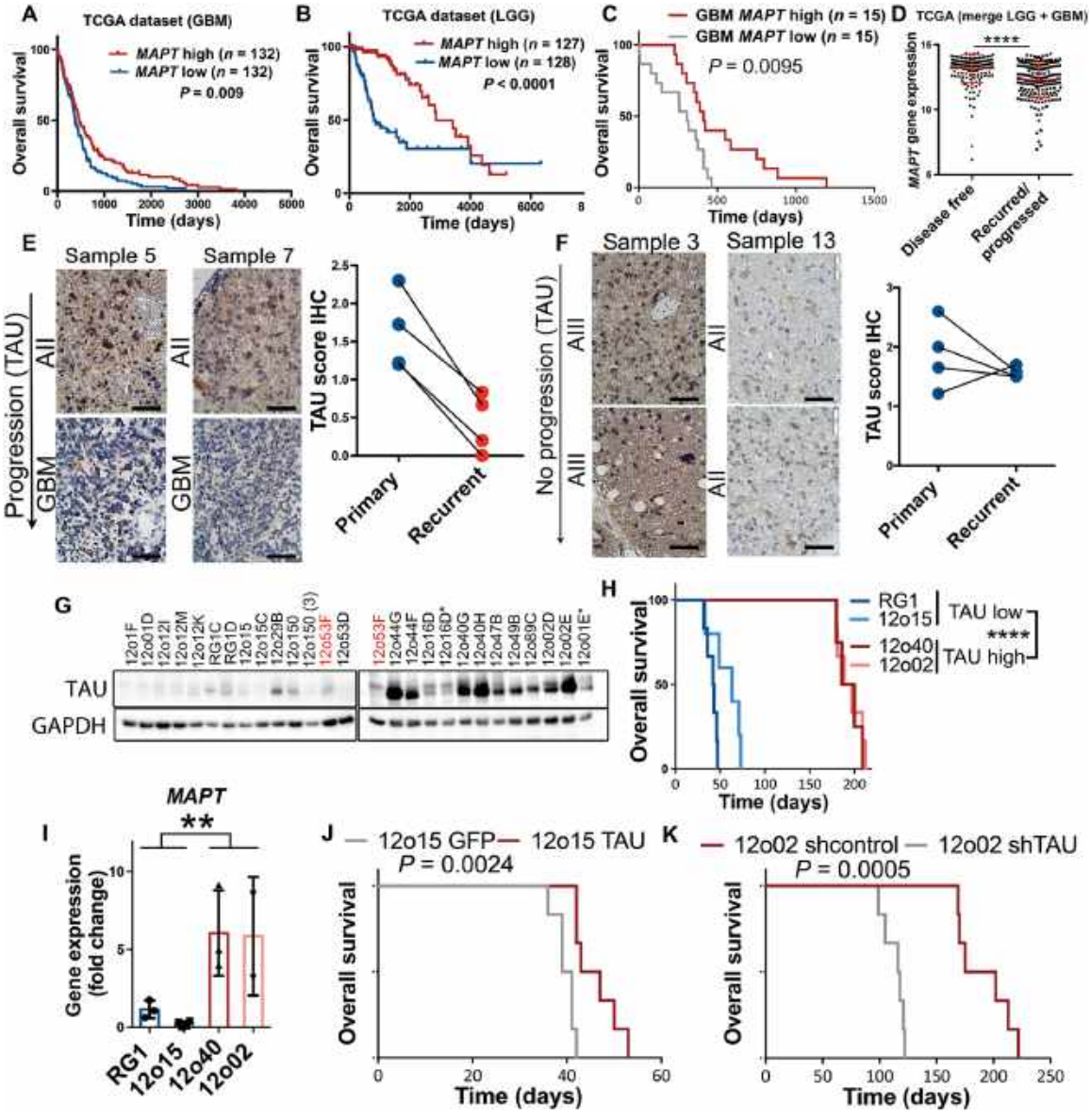

Fig. 2. TAU expression negatively correlates with glioma aggressiveness. (**A** to **C**) Kaplan-Meier overall survival curves of patients from the TCGA GBM cohort ($n = 264$) (A), the TCGA LGG cohort ($n = 155$), and our own GBM cohort ($n = 30$) (C). Patients in each cohort were stratified into two groups based on high and low *MAPT* expression values [RNA-seq in (A) and (B), and qRT-PCR in (C) (*HPRT* was used for normalization)]; log-rank (Mantel-Cox) test. (**D**) Analysis of *MAPT* expression by RNA-seq in gliomas (TCGA cohort) grouped according to the clinical evolution of the tumors ($n = 386$). (**E** and **F**) Representative pictures of the TAU IHC staining of paired glioma samples (primary and recurrent tumor). Average TAU IHC score of the paired samples is shown on the right. (**G**) WB analysis of TAU expression in tumor tissue extracts from subcutaneous PDXs. The same extract from 12o53F cells was loaded in both gels for comparison. GAPDH was used as a loading control. (**H**) Kaplan-Meier overall survival curves of mice that were orthotopically injected with different primary GBM cell lines; log-rank (Mantel-Cox) test. (**I**) qRT-PCR analysis of *MAPT* expression in tumor tissue extracts from (H). *HPRT* was used for normalization. (**J**) Kaplan-Meier overall survival curves of mice that were orthotopically injected with 12o15 cells overexpressing GFP or TAU ($n = 6$). (**K**) Kaplan-Meier overall survival curves of mice that were orthotopically injected with 12o02 control or 12o02-shTAU cells ($n = 6$); log-rank (Mantel-Cox) test. Data are shown as means ± SD; Student's *t* test; $^{**}P \leq 0.01$; $^{****}P \leq 0.0001$. Scale bars, 50 μm.

tumors (Fig. 3G). Moreover, when we treated primary GBM cells with 2-HG, the oncometabolite induced in the presence of IDH mutations, we observed a dose-dependent accumulation of *MAPT* mRNA (Fig. 3H), an effect that was reversed in the presence of azacytidine (AZA) (Fig. 3I). These results suggest that the increase in the methylation of the CpG:26 region, induced by IDH mut proteins, might change the chromosomal insulator topology and the binding of CTCF to the *MAPT* promoter, activating its transcription.

It is well known that *IDH1/2* mutations define a distinct subset of gliomas with a better outcome, whereas the presence of *IDH* wt in LGGs and GBMs defines a subgroup with poor prognosis (fig. S4F). The expression of wt IDH causes hypomethylation at specific loci, so it has been proposed that the production of both 2-HG and α-KG shapes the methylome (*3*). Regarding *MAPT* regulation, we found a negative correlation between its transcription and the expression of wt *IDH1* on the TCGA (Fig. 3J) and the Rembrandt (Fig. 3K)

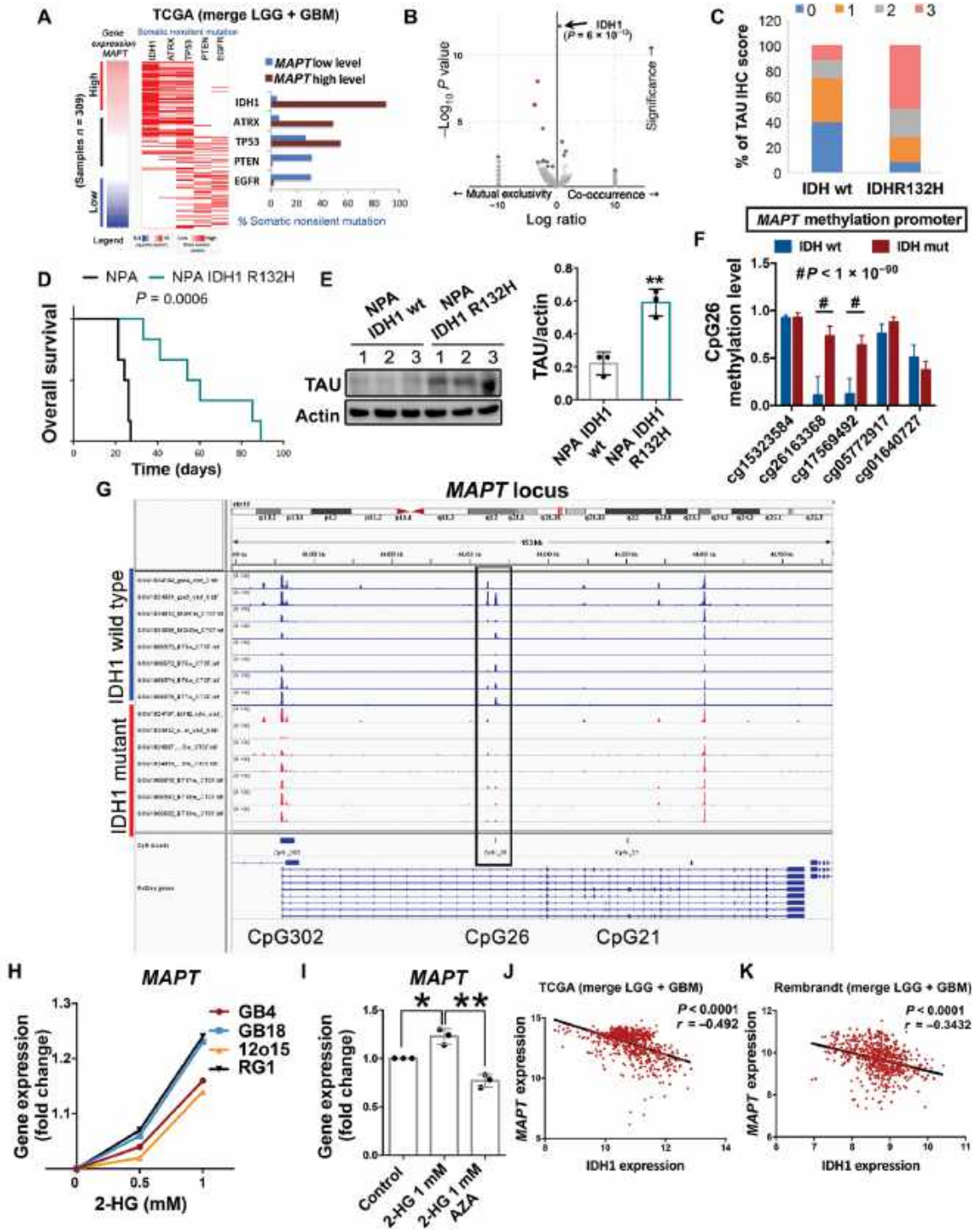

Fig. 3. IDH1/2 function regulates *MAPT* expression. (**A**) Analysis of nonsilent somatic mutations in genes commonly modified in diffuse glioma grouped on the basis of high or low expression of *MAPT*. (**B**) Volcano plots showing mutated genes with differential distribution in glioma comparing tumors with high and low *MAPT*. The arrow points to *IDH1* mutations. (**C**) Percentage of tumors with different TAU IHC score in wt ($n = 35$) and mut ($n = 36$) *IDH1* gliomas. (**D**) Kaplan-Meier overall survival curves of mice that were orthotopically injected with NPA IDH1 wt or NPA IDH1 R132H cells ($n = 6$); log-rank (Mantel-Cox) test. (**E**) WB analysis and quantification of TAU expression in intracranial tumors from (D). Actin was used as loading control. (**F**) Quantification of the methylation of CpG26 using five different probes and comparing IDH wt versus IDH mut gliomas. (**G**) CTCF-binding profiles for the *MAPT* CpG26 locus in IDH mut and IDH wt tumors, normalized by average signal. (**H**) Analysis of the expression of *MAPT* transcription by qPCR in the presence of increasing amounts of 2-hydroxyglutarate (2-HG) in RG1, 12o15, GB4, and GB18 cells. (**I**) Analysis of the expression of *MAPT* transcription by qRT-PCR in RG1 cells cultured in the presence of 1 mM 2-HG, with or without azacytidine (AZA) (1 μM) ($n = 3$). (**J** and **K**) Correlation between the expression of *MAPT* and wt *IDH1* using the TCGA-merge (LGG + GBM) ($n = 669$) (J) and the Rembrandt (LGG + GBM) ($n = 580$) (K) cohorts, Pearson's correlation test. Data are shown as means ± SD; Student's *t* test; $^{*}P \leq 0.05$; $^{**}P \leq 0.01$.

cohorts, suggesting that IDH wt function might inhibit the expression of the *MAPT* promoter.

TAU opposes EGFR signaling in gliomas

To gain insight into the reduction in tumor aggressiveness by *MAPT*, we performed a DAVID gene ontology analysis (a functional annotation clustering tool) to search for the pathways co–up-regulated with this gene in gliomas. As expected, we found a positive association between *MAPT* expression and microtubule- and neurogenic-related processes. Other TAU-linked pathways were related to receptor tyrosine kinase signaling (fig. S5A). In addition, our in silico analysis indicated that *IDH* mutations, which accumulate in the *MAPT*-high gliomas, are mutually exclusive with *EGFR* and *PTEN* (phosphatase and tensin homolog) mutations (Figs. 3A and 4A and fig. S5B), which was confirmed in a volcano plot analysis (Fig. 4B). To interrogate whether TAU could be modulating this signaling pathway, we expressed green fluorescent protein (GFP) (control), IDH wt, or IDH R132H in an EGFR-amplified cell line (RG1). As we have previously observed in the mouse glioma model (Fig. 3D), cells overexpressing IDH mut were less aggressive than cells overexpressing IDH wt when they were injected in the brains of immunodeficient mice (Fig. 4C). This effect was paralleled by changes in the quantity of TAU, which augmented in IDH mut and decreased in IDH wt tumors, compared with gliomas generated by GFP-expressing cells (Fig. 4, D and E). These results are in agreement with the in silico data (Fig. 3, J and K) and suggest that the induction of *MAPT* transcription might depend on the balance between wt and mut IDH functions. The phosphorylation of EGFR showed a negative correlation with the quantity of TAU in mouse tumors (Fig. 4, D and F) and in human samples (fig. S5, C and D). The expression of *MAPT* correlated with overall survival in the group of *EGFR*amp/wt gliomas (Fig. 4G), but it had no clinical relevance in the presence of additional mutations in *EGFR* (Fig. 4H). Together, these results highlight that there might be a negative effect of IDH/TAU on the pathway activated by this receptor, but only in the group of *EGFR*amp/wt gliomas.

To evaluate the effect of TAU on EGFR signaling, we overexpressed this protein in two mouse glioma models: SVZ-EGFRamp/wt and SVZ-EGFRvIII, and we analyzed their capacity to grow as intracranial allografts. These models were generated by transforming subventricular zone (SVZ) progenitors from p16/p19 knockout (ko) mice with retrovirus expressing either the wt or the variant III (vIII) isoform of the receptor. Both types of cells depend on EGFR signaling in vitro and in vivo, and they generate gliomas with a high penetrance. Overexpression of TAU inhibited the growth of SVZ-EGFRamp/wt mouse gliomas (Fig. 4I), but it had no effect on SVZ-EGFRvIII tumors (Fig. 4J). Similar results were obtained when we overexpressed this protein in two human primary cell lines, RG1 (*EGFR*amp) and 12o150 (*EGFR* amplified and mutated, *EGFR*mut). TAU impaired the growth of the first (Fig. 4K), but it had no effect on the second (Fig. 4L). However, TAU did not inhibit the survival or the self-renewal capacity of the mouse (fig. S5, E and F) or the human (fig. S5, G and H) glioma cells in vitro, suggesting that the consequence of the overexpression of this protein on the EGFR signaling pathway might be relevant only in the context of the tumor microenvironment (TME).

Microtubule stabilizers, like TAU and epothilone D, favor the degradation of wt EGFR

To study how TAU could modulate EGFR signaling, we first performed a WB analysis of the dissected tumors. We observed that the amount of phospho-EGFR was attenuated in SVZ-EGFRamp/wt tumors (Fig. 5A) as well as in *EGFR*amp xenografts (Fig. 5B), whereas there was no change in SVZ-EGFRvIII gliomas (Fig. 5C) or in *EGFR*mut xenografts (Fig. 5D) after TAU overexpression. These data reinforce the notion that TAU opposes wt but not mut EGFR signaling.

Previous results from our group have demonstrated that, as a result of TAU function, stabilized microtubules become heavily acetylated through the inhibition of histone deacetylase 6 (HDAC6). The increase in tubulin acetylation can serve as a readout of TAU expression (*17*). Moreover, it has been proposed that this acetylation promotes the subsequent degradation of EGFR due to changes in the microtubule-dependent endocytic machinery (*18*). In agreement with these published data, we observed a higher quantity of acetylated tubulin in TAU-overexpressing gliomas, which were paralleled by a strong decrease in the amount of total EGFR protein (Fig. 5E). The down-regulation of EGFR protein was also observed in vitro after TAU lentiviral induction and was reverted in the presence of chloroquine (lysosome inhibitor) (Fig. 5F). Therefore, the results suggest that TAU might impair EGFR signaling through the stabilization of the microtubules and the subsequent alteration of the receptor trafficking, which would lead to its degradation. To validate this hypothesis, we treated RG1 (*EGFR*amp)–injected mice with a taxol derivative, epothilone D (EpoD). This molecule can also stabilize the microtubules. EpoD has been proved to reach the brain and revert some of the axonal defects of a TAU loss-of-function model (*19*). Systemic treatment with EpoD substantially delayed RG1 tumor formation (Fig. 5G) and reduced phospho-EGFR in the tumors (Fig. 5, H and I) without changing the quantity of TAU protein (Fig. 5, H and I). This was accompanied by a strong down-regulation of EGFR and a clear increase in the amount of acetylated tubulin (Fig. 5, H and I). Together, our data support the notion that the microtubule-related function of TAU is responsible for its effect on EGFR signaling and tumor growth in gliomas. Moreover, they suggest that taxol derivatives could reduce the aggressiveness of gliomas. We observed that EpoD treatment not only increased the survival of mice injected with SVZ-EGFRamp/wt cells but also made those tumors more sensitive to chemotherapy (Fig. 5J), so there could be a therapeutic opportunity for the use of these compounds in patients with glioma.

TAU blocks the mesenchymalization of EGFRamp/wt glioma cells

Bioinformatic analysis of LGGs and GBMs from the TCGA dataset showed that the amount of *MAPT* mRNA correlated positively with the PN signature, whereas it exhibited a strong negative correlation with the MES profile of gliomas (Fig. 6A and fig. S6, A to F). In addition, we observed that *MAPT* transcription negatively correlated with the expression of the NF-κB pathway and the inflammatory signature, but not with other signatures, like those associated with hypoxia or PDGFRα (Fig. 6, A and B). These in silico observations were confirmed by the WB analysis of RG1 (EGFRamp) xenografts, which showed that overexpression of TAU inhibited NF-κB subunit phosphorylation and reduced the amount of TAZ protein, a master regulator of the MES phenotype (Fig. 6, C and D) (*20*). Similar results were obtained in the WB analysis of 12o15 xenografts (Fig. 6, E and F), a primary cell line that overexpresses the receptor in the absence of gene amplification (*21*). TAU did not change the transcription of other MES genes (Fig. 6G), and it had no effect on TAZ or NF-κB activation in *EGFR*mut tumors (fig. S6G).

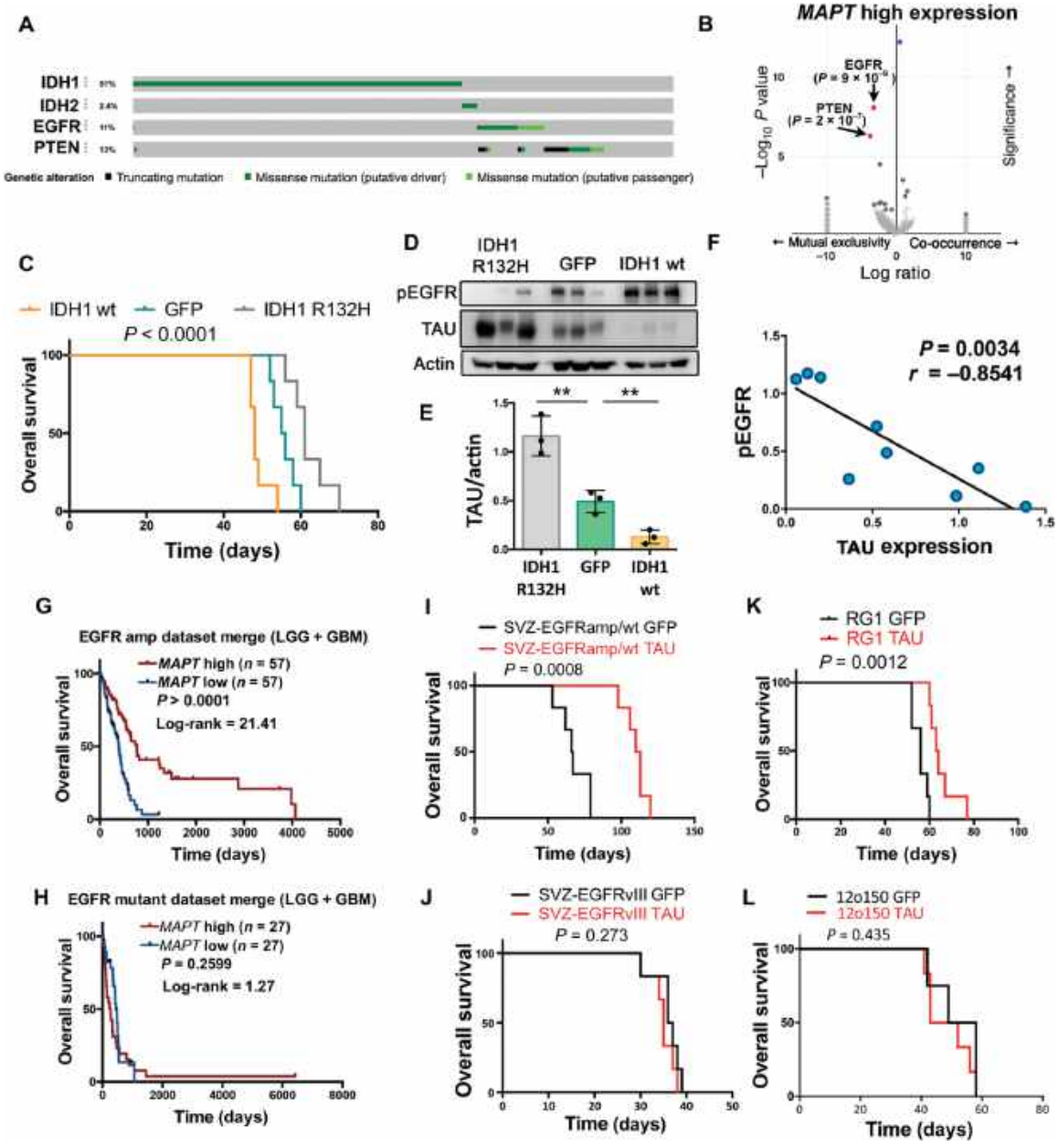

Fig. 4. TAU opposes EGFR in gliomas. (**A**) Distribution of somatic nonsilent mutations in *IDH1/2*, *EGFR*, and *PTEN* in a glioma cohort (TCGA, $n = 812$). (**B**) Volcano plots showing mutated genes with differential distribution in gliomas, comparing tumors with high and low *MAPT*. The arrows point to *PTEN* and *EGFR* mutations. (**C**) Kaplan-Meier overall survival curves of mice that were orthotopically injected with RG1, RG1 IDH1 wt, or RG1 IDH1 R32H cells ($n = 6$); log-rank (Mantel-Cox) test. (**D**) WB analysis of phosphorylated EGFR (pEGFR) and TAU in intracranial tumors from (C). Actin was used as a loading control. (**E**) Quantification of the amount of TAU in (D). (**F**) Correlation between TAU and pEGFR in RG1 tumors, Pearson's correlation test. (**G** and **H**) Kaplan-Meier overall survival curves of patients from the LGG + GBM TCGA cohort. Patients were separated on the basis of the *EGFR* status: tumors without mutations (amplified or wt) ($n = 114$) (G) and amplified tumors with mutations ($n = 54$) (H). Then, they were stratified into two groups based on *MAPT* expression values; log-rank (Mantel-Cox) test. (**I** to **L**) Kaplan-Meier overall survival curves of mice that were orthotopically injected with SVZ-EGFRamp/wt (I), SVZ-EGFRvIII (J), RG1 (*EGFR*amp) (K), or 12o150 (*EGFR*mut) (L) cells, overexpressing either GFP or TAU ($n = 6$); log-rank (Mantel-Cox) test. Data are shown as means ± SD; Student's *t* test; $^{**}P \leq 0.01$.

TAU overexpression also induced the transcription of *OLIG2* (Fig. 6H), a gene that is frequently used as a bona fide PN marker (*22*). Moreover, the immunofluorescence (IF) analysis of RG1 gliomas confirmed that TAU repressed nuclear TAZ while inducing nuclear OLIG2 in the tumor cells (Fig. 6I). These data were confirmed by RT-PCR analysis of human samples (Fig. 6, J and K) and by in silico studies (fig. S6H), which showed that *MAPT* negatively correlated with *TAZ* and positively with *OLIG2* expression. Together, our results indicate that TAU induces a change in the glioma phenotype, repressing MES regulators and inducing PN promoters in the tumor cells through the regulation of the EGFR/TAZ/NF-κB pathway. It is important to remark that TAU did not change the tumor burden of

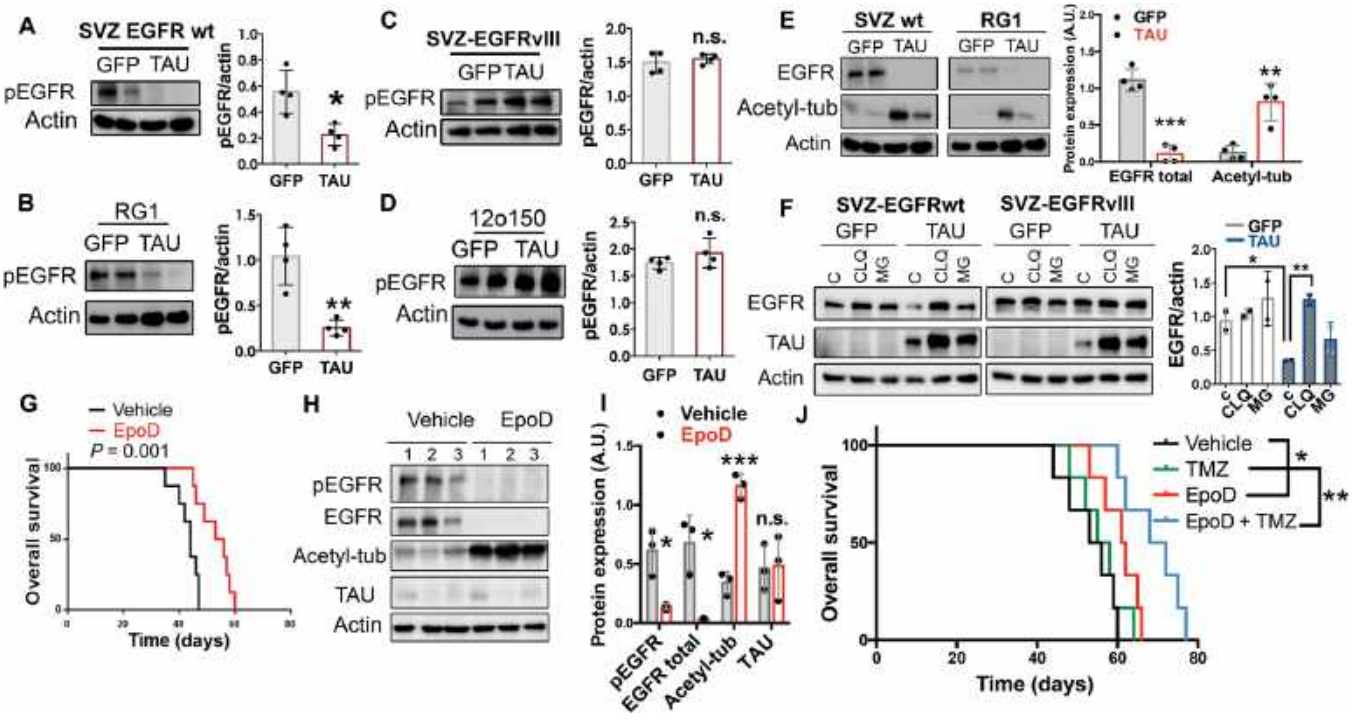

Fig. 5. Microtubule-stabilizing molecules impair EGFRwt stability and signaling in gliomas. (**A** to **D**) WB analysis and quantification of pEGFR in SVZ-EGFRamp/wt (A), RG1 (B), SVZ-EGFRvIII (C), and 12o150 (D) tumors after the overexpression of GFP or TAU. Actin was used as a loading control. (**E**) WB analysis and quantification of total EGFR and acetylated tubulin (Acetyl-tub) in SVZ-EGFRamp/wt and RG1 tumors after the overexpression of GFP or TAU. Actin was used as a loading control. (**F**) WB analysis of total EGFR in SVZ-EGFRamp/wt and SVZ-EGFRvIII cells after the overexpression of GFP or TAU, in the absence (Control, C) or in the presence of MG123 (MG, 10 μM) and chloroquine (CLQ, 200 μM). Quantification of the WB of SVZ-EGFRamp/wt cells is shown on the right. (**G**) Kaplan-Meier overall survival curves of mice that were orthotopically injected with RG1 cells and subsequently treated with intraperitoneal injections (twice per week) of EpoD (1 mg/kg) ($n = 8$); log-rank (Mantel-Cox) test. (**H** and **I**) WB analysis (H) and quantification (I) of pEGFR, total EGFR, Acetyl-tub, and TAU in the tumors (G). Actin was used as loading control. (**J**) Kaplan-Meier overall survival curves of mice that were orthotopically injected with SVZ-EGFRamp/wt cells and subsequently treated with intraperitoneal injections (twice per week) of EpoD (1 mg/kg) and/or temozolomide (TMZ) (5 mg/kg per day) ($n = 6$); log-rank (Mantel-Cox) test. Data are shown as means ± SD; Student's *t* test; $^{*}P \leq 0.05$, $^{**}P \leq 0.01$, $^{***}P \leq 0.001$. A.U., arbitrary units.

RG1 cells in the presence of TAZ overexpression (Fig. 6, L and M), which highlights that TAU likely inhibits the growth of EGFRamp/wt glioma growth by blocking the transdifferentiation capacity of tumor cells and the appearance of MES features.

Previous results from our group and others have shown that, in comparison with PN cancer stem cells (CSCs), MES CSCs are more capable of glioma initiation, probably due to their increased angiogenic capacity (*23*, *24*). In agreement with this observation, the overexpression of TAU in RG1 cells impaired their capacity to form subcutaneous xenografts (fig. S7, A and B). Furthermore, we found that most of the genes up-regulated with TAZ in gliomas were associated with angiogenesis and tumor vasculature (fig. S7, C to F). Particularly, we noticed that markers of pericytes, which are considered as perivascular MES stem cells (*25*), were among the genes, which correlated better with TAZ in gliomas (fig. S7, G and H). To examine whether this transcription factor could modulate the function and/or the number of mural cells, we expressed shTAZ in RG1 cells and we performed an orthotopic in vivo experiment. The knockdown of this gene clearly reduced the aggressiveness of the tumors (Fig. 6N) and inhibited the expression of several pericyte markers (Fig. 6O). It is worth mentioning that TAZ seems to regulate pericytic differentiation in a cell-autonomous way as we also observed a reduction in these markers after the in vitro lentiviral induction of shTAZ in RG1 and 12o15 cells (Fig. 6, P to R). These results are in agreement with recent publications showing that most of the pericytic functions in GBM are performed by the highly plastic CSCs, which undergo a transdifferentiation process, acquiring MES and mural cell features (*26*–*28*).

TAU reduces the amount of tumor-derived pericytes and normalizes the vasculature of EGFRamp gliomas

Our results indicate that TAU impairs the switch to MES phenotype of glioma cells by blocking the expression of TAZ, which is induced in response to EGFR activation. Moreover, we could hypothesize that, as a result of this inhibition, the capacity of the tumor cells to transdifferentiate into pericytes might be reduced. Therefore, we analyzed the vascular component of RG1 (EGFRamp) tumors after the overexpression of TAU. We observed a marked decrease in the number of αSMA (α-smooth muscle actin)– and CD248-positive cells (Fig. 7A), together with the blockade of the transcription of human pericytic markers in TAU-expressing tumors (Fig. 7B). A similar result was observed in 12o15 (EGFRwt) (fig. S8A), but not in 12o150 (EGFRmut) xenografts (fig. S8B). TAU did not impair the transcription of mouse pericytic genes (Fig. 7C), reinforcing the idea that this protein might inhibit the glioma-to-pericyte transdifferentiation without altering the quantity and/or the differentiation capacity of host pericytes.

The IF analysis of the tissues also revealed that there was a substantial inhibition of cellular proliferation (fig. S8, C and D) after TAU overexpression, accompanied by a decrease in the number of

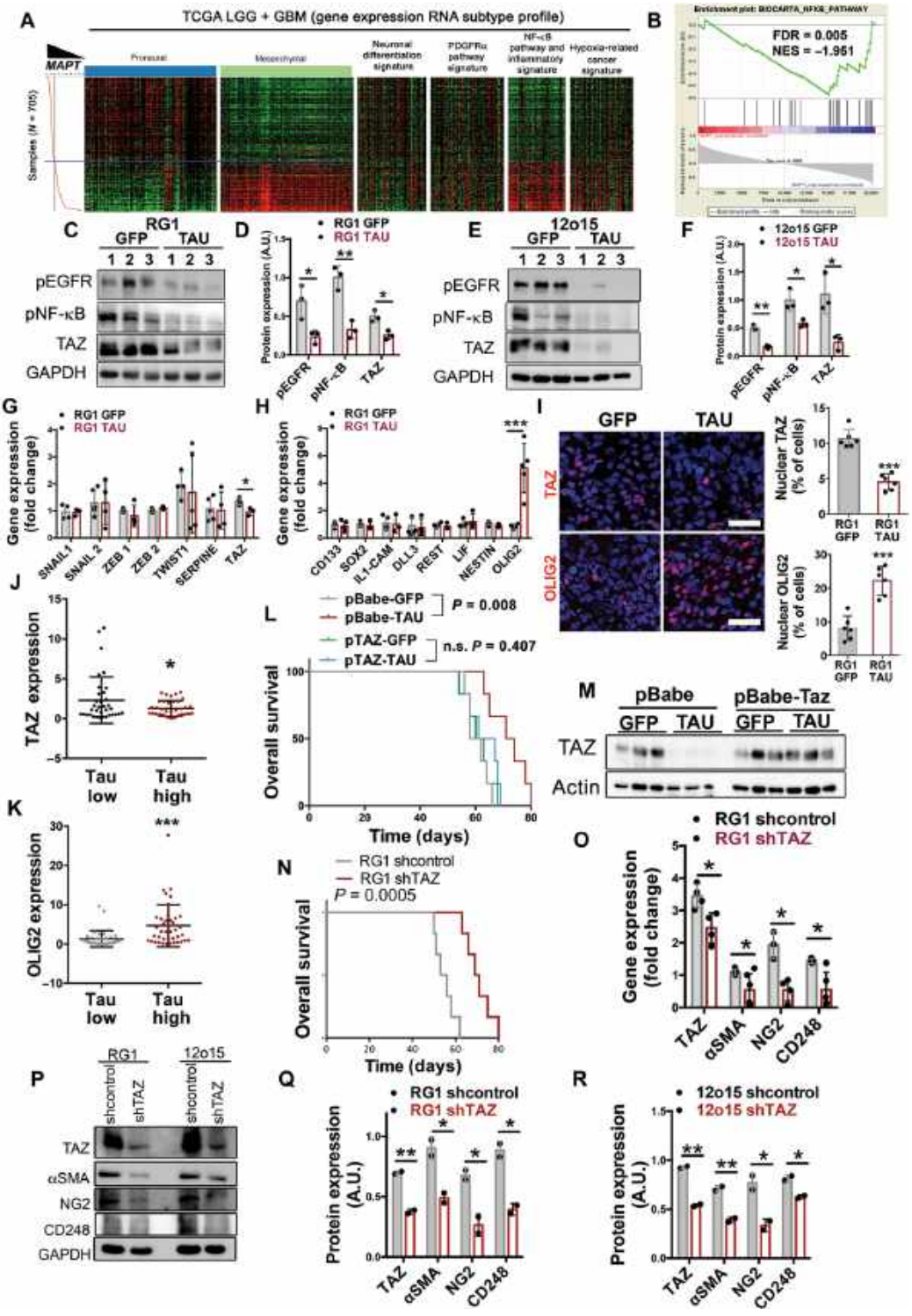

Fig. 6. TAU blocks the MES features of *EGFR*amp/wt cells through the inhibition of the EGFR/NF-κB/TAZ axis. (**A**) Heatmap of PN, MES, neuronal differentiation, PDGFRα pathway, NF-κB/inflammation, and hypoxia-related cancer expression genes depending on *MAPT* expression. (**B**) GSEA (gene set enrichment analysis) enrichment plot analysis using *MAPT* gene expression values as template and the NF-κB pathway gene set from the Biocarta pathways database. (**C** to **F**) WB analysis (C and E) and quantification (D and F) of pEGFR, phosphorylated pNF-κB (p65) and TAZ in RG1 (C and D) and 12o15 (E and F) xenografts expressing either GFP or TAU. GADPH was used as a loading control ($n = 3$). (**G** and **H**) qRT-PCR analysis of MES (G)– and PN subtype (H)–related genes in RG1 xenografts expressing GFP or TAU. *HPRT* was used for normalization. (**I**) Representative images of TAZ (top) or OLIG2 (bottom) IF staining of sections from GFP- or TAU-overexpressing RG1 gliomas. Quantification is shown on the right. (**J** and **K**) qRT-PCR analysis of *TAZ* (J) and *OLIG2* (K) in gliomas ($n = 6$). Tumors were classified in two groups based on the expression of *MAPT* ($n = 72$). *HPRT* expression was used for normalization. (**L**) Kaplan-Meier overall survival curves of mice that were orthotopically injected with RG1 cells overexpressing GFP, TAU or GFP, and TAU plus TAZ ($n = 6$); log-rank (Mantel-Cox) test. (**M**) WB analysis of TAZ in the tumors (L). Actin was used as loading control. (**N**) Kaplan-Meier overall survival curves of mice that were orthotopically injected with RG1 shcontrol or RG1 shTAZ cells ($n = 6$); log-rank (Mantel-Cox) test. (**O**) qRT-PCR analysis of pericytic-related genes in the tumors (N). (**P** to **R**) WB analysis (P) and quantification (Q and R) of TAZ, αSMA, NG2, and CD248 in RG1 (P and Q) or 12O15 (P and R) cells after *TAZ* downregulation. GADPH was used for normalization. Data are shown as means ± SD; Student's *t* test; $^{*}P \leq 0.05$; $^{**}P \leq 0.01$; $^{***}P \leq 0.001$. Scale bars, 25 μm.

dilated blood vessels (Fig. 7, D and E), typical of malignant gliomas (*29*). The angiogenic signals that are reduced upon TAU induction are likely to derive, at least in part, from the tumor cells, as the supernatant of RG1 cells overexpressing TAU showed a reduced capacity to induce HMBEC (human brain microvascular endothelial cells) sprouting (Fig. 7F) and contained less VEGF (vascular endothelial growth factor) (Fig. 7G).

To further characterize the phenotype induced by TAU, we analyzed several vascular-related parameters in the tumor tissues. We observed a reduction in the extravasation of immunoglobulin G (IgG)

after TAU overexpression (Fig. 7H), which indicates that these tumors present a less aberrant tumor vasculature, with an increase in the integrity of the blood-brain barrier (BBB), compared with the controls. In agreement with this hypothesis, TAU induced a clear reduction in the quantity of Ang2 (angiopoietin 2) (Fig. 7I), a key regulator of angiogenesis that has been associated with vascular abnormalities in glioma, acting as an antagonist of Ang1 (*30*). We observed a strong decrease in the *Ang2/Ang1* ratio after TAU overexpression in the *EGFR*amp model (Fig. 7J), but not in the *EGFR*mut xenografts (fig. S8E). These results suggest that the transdifferentiation of glioma cells into MES/pericyte-like cells, induced by EGFR signaling, favors the secretion of angiogenic signals and the formation of an aberrant vasculature. This process can be impaired by TAU in EGFRwt/amp, but not in EGFRmut gliomas.

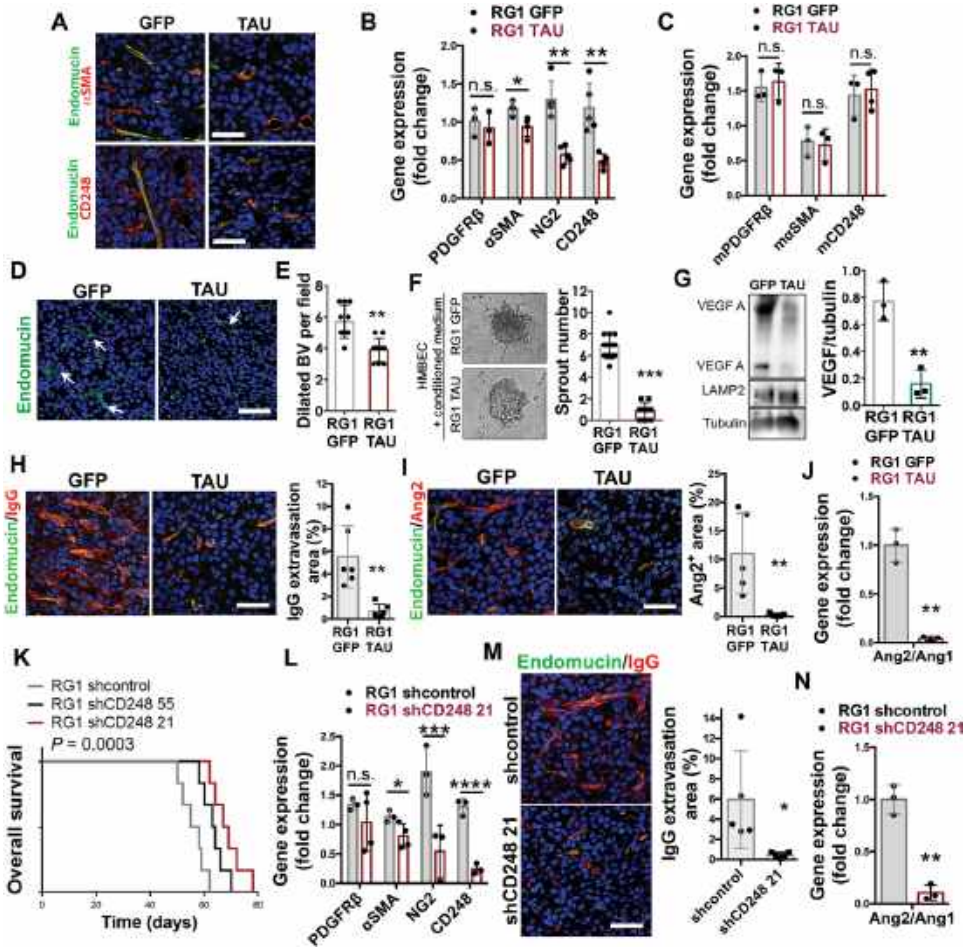

Fig. 7. TAU overexpression blocks the appearance of tumor-derived pericytes in *EGFRwt*/amp gliomas, inhibiting angiogenesis and normalizing the tumor vasculature. (**A**) Representative images of IF costaining of endomucin and αSMA (top) or endomucin and CD248 (bottom), on sections from RG1 xenografts expressing GFP or TAU. (**B**) qRT-PCR analysis of pericytic-related genes (using human-specific primers) in RG1 GFP and TAU xenografts. *HPRT* was used for normalization. (**C**) qRT-PCR analysis of pericytic-related genes (using mouse-specific primers) in RG1 GFP and TAU xenografts. Actin was used for normalization ($n = 3$ to 5). (**D**) Representative images of endomucin IF staining of sections from RG1 xenografts expressing GFP or TAU. (**E**) Quantification of dilated blood vessels (BV) (indicated by arrows) in (D) ($n = 10$). (**F**) Representative phase-contrast images of HMBEC cells cultured in the presence of conditioned media from RG1 GFP or RG1 TAU cells. The number of sprouts is shown on the right. (**G**) WB and quantification of VEGF in the supernatant of RG1 cells after overexpression of GFP or TAU. LAMP2 and tubulin were used as loading controls. (**H**) Representative images of IF costaining of endomucin and IgG on sections from RG1 xenografts expressing GFP or TAU. Quantification is shown on the right. (**I**) Representative images of IF costaining of endomucin and Ang2 sections from RG1 xenografts expressing GFP or TAU. Quantification is shown on the right. (**J**) Ratio of *Ang2/Ang1* expression measured by qRT-PCR in RG1 gliomas after TAU overexpression ($n = 3$). Actin was used for normalization. (**K**) Kaplan-Meier overall survival curves of mice that were orthotopically injected with RG1 cells expressing shcontrol, shCD248 55, or shCD248 21 ($n = 6$); log-rank (Mantel-Cox) test. (**L**) qRT-PCR analysis of pericytic-related genes in RG1 tumors expressing shcontrol or shCD248 21 ($n = 3$ to 4). (**M**) Representative images of IF costaining of endomucin and IgG from tumors in (K). Quantification is shown on the right. (**N**) Ratio of *Ang2/Ang1* expression measured by qRT-PCR in RG1 gliomas after *CD248* down-regulation ($n = 3$). Actin was used for normalization. Data are shown as means ± SD; Student's *t* test; $^*P \le 0.05$; $^{**}P \le 0.01$; $^{***}P \le 0.001$; $^{****}P \le 0.0001$. Scale bars, 25 μm.

To confirm the relevance of the tumor-derived pericytes in the growth of EGFRamp gliomas, we down-regulated *CD248* expression in RG1 cells. CD248 (endosialin) aids in supporting tumor microvasculature, and it is expressed in pericytes, especially in malignant solid tumors, including high-grade gliomas (*27*, *31*). We confirmed the down-regulation of *CD248* mRNAs with two of these short hairpin RNA (shRNA) sequences (fig. S8F), and we injected those interfered cells into the brains of immunodeficient mice in the presence of normal host pericytes. We observed a substantial delay in tumor growth after *CD248* down-regulation (Fig. 7K). Moreover, the inhibition of *CD248* in the tumor cells reduced the expression of other pericytic markers in vitro (fig. S8G) and in vivo (Fig. 7L), reinforcing the role of this molecule in the transdifferentiation of tumor cells into pericytes. Furthermore, tumors formed after *CD248* down-regulation showed a reduction in the extravasation of IgG (Fig. 7M), as well as a decreased *Ang2/Ang1* ratio (Fig. 7N), which further support the hypothesis that the depletion of tumor-derived pericytes (at least in EGFRwt/amp tumors) normalizes the glioma vasculature and reduces the aggressiveness of these gliomas.

TAU expression is a surrogate marker of the less aggressive vascular behavior of gliomas

The data presented so far place TAU at the boundary between the most common genetic alterations of gliomas (those that affect *IDH1/2* and *EGFR*) and the regulation of the TME, in particular the vascular phenotype. To translate the results into the clinical settings, we used our own cohort of patient samples (qRT-PCR analysis) and the data from the TCGA (in silico analysis). We divided the tumors into an IDH1 mut (those with higher transcription of *MAPT*) and an IDH1 wt group, and we subclassified the second one into high- or low-TAU gliomas

(Fig. 8, A and B). We confirmed the negative correlation between *MAPT* expression and phospho-EGFR (Fig. 8C and fig. S9A) and between the transcription of *CD248* and *MAPT* (Fig. 8, D and E, and fig. S9B), which was confirmed by the IHC analysis of the tumors. The representative images in Fig. 8F evidence the gradual normalization of the vasculature in parallel with the increase in TAU staining (Fig. 8F). Furthermore, the quantification of the CD248 score (Fig. 8G), the transcription of *CD34* (Fig. 8H), and the amount of dilated vessels (Fig. 8I) confirmed the visual differences and reinforced our model, in which TAU expression might be used as a surrogate marker of the less aggressive vascular behavior in gliomas.

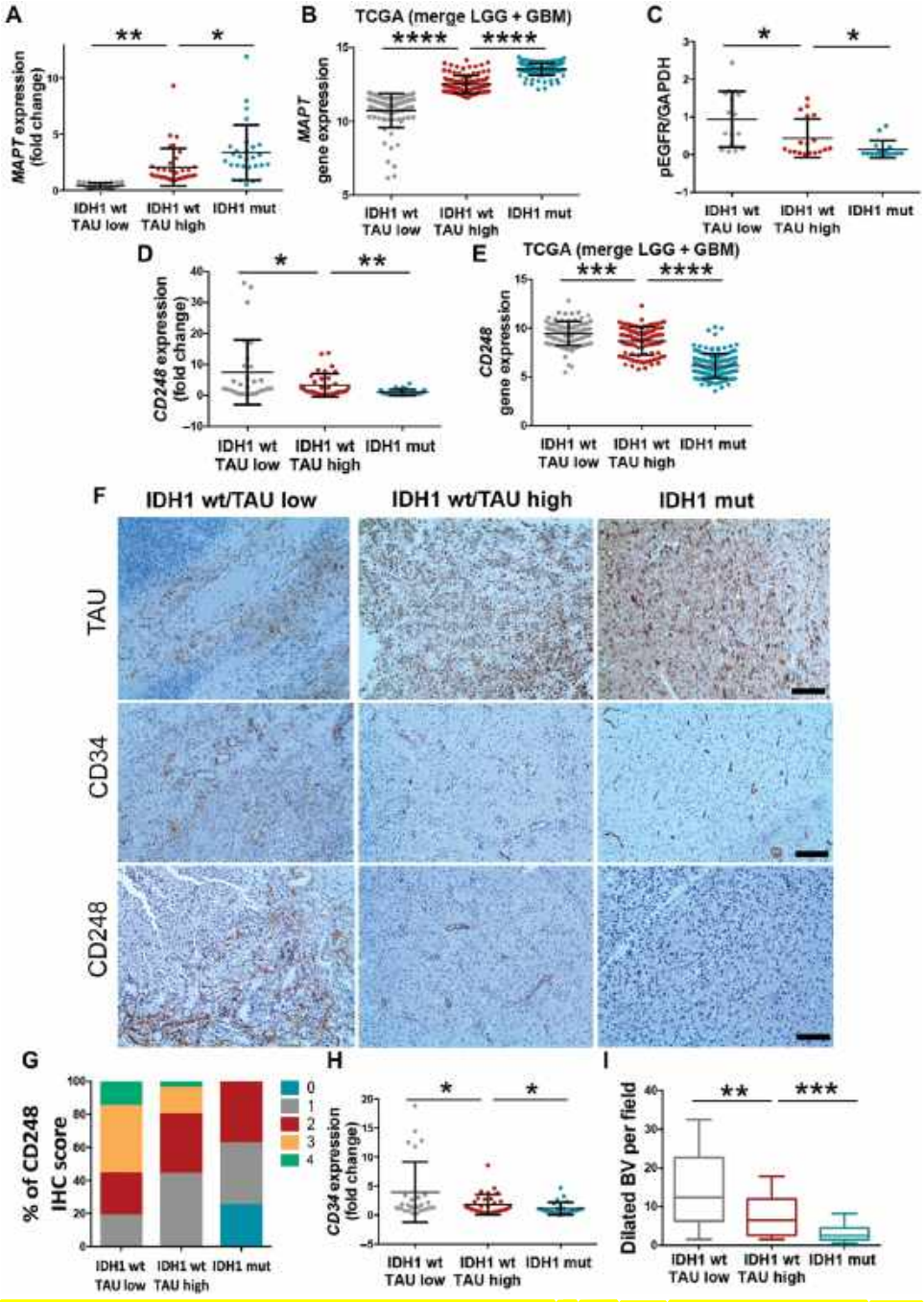

Fig. 8. Analysis of TAU and vascular molecules in human samples. (**A** to **E**) *MAPT* (A and B), pEGFR (C), and *CD248* (D and E) expression was determined by qRT-PCR analysis (glioma cohort) ($n = 87$) (A and D), RNA-seq analysis (TCGA–LGG + GBM cohort) ($n = 319$) (B and E), or by WB ($n = 50$) (C). Tumors were classified into three groups: IDH1 wt (TAU low), IDH1 wt (TAU high), and IDH1 mut. *HPRT* and GAPDH expression was used for normalization. (**F**) Representative pictures of the IHC staining of TAU, CD34, and CD48 in three tumors, one for each of the groups. (**G**) Percentage of tumors with different CD248 IHC score in (F) ($n = 68$). (**H**) *CD34* transcription was determined by qRT-PCR analysis (GBM cohort) ($n = 87$). (**I**) Quantification of the dilated blood vessels in (F) ($n = 68$). Data are shown as means ± SD; Student's *t* test; $^{*}P \leq 0.05$; $^{**}P \leq 0.01$; $^{***}P \leq 0.001$; $^{****}P \leq 0.0001$. Scale bars, 100 μm.

DISCUSSION

IDH1/2 mutations identify a genetically and clinically distinct glioma entity. Patients with such tumors have a much better prognosis (independently of histology), and they show improved responses to chemotherapy and/or irradiation (*32*, *33*). The reexpression of IDH1 R132H in GBM cells can reduce tumor growth (*14*, *34*). However, the molecular basis for the tumor suppressor functions of IDH mutations is unclear. Here, we have identified TAU, a known microtubule stabilizer, as a new epigenetic target of IDH mut in gliomas. On the basis of our findings, we suggest that these mut enzymes, acting through the increase in *MAPT* transcription, favor the normalization of the vasculature and impede the progression of the disease (fig. S10). TAU down-regulation induced a marked increase in tumor burden in the orthotopic xenograft mouse models. Moreover, the longitudinal analysis of a set of paired samples showed that the quantity of TAU decreases as LGGs evolve into higher-grade lesions. IDH1/2 status seems to be consistent during glioma progression (*35*, *36*), suggesting the existence of specific mechanisms that might be inhibiting *MAPT* transcription in the recurrent tumors. One possible explanation would be that an increase in wt IDH protein in the recidives could impair TAU expression, as it happens in the mouse xenografts. It has been recently shown that the nonmutated IDH1 is up-regulated in primary GBM in comparison with secondary GBM or LGG, where it promotes aggressive growth and therapy resistance (*5*).

IDH1/2 mutations represent early events in the process of tumorigenesis (*37*). Many studies have shown that the presence of these mutated proteins induce important metabolic and epigenomic changes, which could explain their oncogenic properties (*4*, *14*, *15*, *38*, *39*). Several inhibitors have been developed

to block IDH mut function in different cancers. Some of them have shown antitumor activity in mouse glioma models (*40*), and they have been approved to be tested in IDH mut patients (*41*). However, the tumor suppressor functions of these proteins in gliomas, including the vascular normalization that we have described here, could represent a severe pitfall for these approaches. The treatment with IDH mut inhibitors has been associated with a radioprotective effect (*42*) and a decreased sensitivity to cisplatin (*43*). Regarding IDH wt gliomas, our results suggest that microtubule stabilizers could imitate TAU function and reduce the aggressiveness of the tumors, which could render them sensitive to conventional chemotherapy (Fig. 5I). The same compounds could be tested in combination with IDH mut inhibitors in LGG in an attempt to impair tumor growth and, at the same time, block the transformation into more aggressive tumors.

Our results indicate that TAU is a key inhibitor of wt EGFR signaling in gliomas. Accordingly, drugs that interfere with microtubule function have been associated with EGFR inactivation in other cancers (*44*), as they seem to alter endocytic trafficking (*11*). Moreover, it has been shown that microtubule acetylation, which is promoted by TAU function (*17*), promotes the degradation of EGFR through changes in the microtubule-dependent endocytic trafficking (*18*). We propose that a similar mechanism could be operating in gliomas, but only in the absence of EGFR mutations. In that sense, EGFR mut proteins, especially the vIII isoform, have been associated with the maintenance of the signal in the absence of ligands (*45*), possibly due to changes in the turnover of the mut receptor (*46*). Moreover, it has been proposed that some of the EGFR downstream targets, like NF-κB, become constitutively activated in GBM after vIII expression (*47*). The data presented here further support that EGFR mutations induce a constitutive activation of NF-κB, which would be insensitive to microtubule modulators.

Downstream of EGFR/NF-κB signaling, we have found that TAU overexpression severely reduced the amount of TAZ in GBM. TAZ is a transcriptional coactivator that plays a prominent role in gliomas (*48*), controlling the MES signature (*20*). Moreover, TAZ is induced by NF-κB activation in gliomas and promotes radioresistance (*20*). It has been recently proposed that *TAZ* promoter is a direct target of NF-κB (*49*), so TAU could be inhibiting indirectly the transcription of the *TAZ* gene. However, we cannot discard a possible regulation of the protein stability downstream of EGFR/NF-κB signaling.

Extravasation of the contrast agent gadolinium, measured with T1-weighted magnetic resonance imaging sequences, is used to diagnose high-grade gliomas because it identifies tumors with a compromised BBB. It is well known that IDH mut gliomas are characterized by a lesser extent of contrast enhancement than wt tumors, even if we only consider the group of GBM (*50*). However, the molecular explanation for this behavior was still missing. Our results show that TAU, acting downstream of IDH mut, could normalize the blood vessels and reduce the BBB leakage. These changes could cooperate or even precede other alterations observed in the TME of IDH mut gliomas, like the absence of microthrombi (*51*), as well as the decrease in necrosis areas (*50*) and hypoxia-induced angiogenesis (*52*). Moreover, the immune component and its pro- or antitumoral properties could also be affected by the vascular phenotype of IDH mut gliomas (*53*), explaining the decrease in the immune infiltrate observed in mouse models and human samples (*34*). Future experiments are warranted to decipher the participation of TAU in these other phenotypes.

Although cancer and neurodegenerative diseases are considered as opposite phenomena, there could be a positive association between AD prevalence and GBM incidence (*12*). In AD and other TAUopathies, there is an accumulation of TAU aggregates (gain of toxic function). However, this aggregation of TAU compromises its microtubule-stabilizing functions (loss of physiological function), favoring the evolution of the pathology. In agreement with the loss-of-function model, we have reported behavioral changes and neurogenesis in aged TAU ko mice (*54*). EMT genes are enriched in the affected areas of AD brains (*55*). Moreover, there is an important neurovascular dysfunction at early stages of AD, associated with BBB breakdown and inflammation (*56*), which could be linked to pericyte loss (*57*). Although there is still missing evidence of the relevance of TAU (especially the astrocytic TAU) in these phenotypes, it is tempting to speculate that the loss of function of this protein could represent a link between the progression of the two types of brain diseases. If this hypothesis is correct, targeting pericytes or the MES transdifferentiation of the astrocytes could be an interesting therapeutic approach to be tested in several neurological disorders. Moreover, it would be worth studying whether AD-related drugs could be repurposed to treat brain tumors. In that sense, we have demonstrated that EpoD, a microtubule-stabilizing agent that reduces AD pathology in mouse models (*19*), slows down in vivo glioma growth without any apparent secondary effect. Another second-generation taxane, cabazitaxel, has demonstrated a good antiglioma activity in preclinical tests (*58*) and is being evaluated as a cytotoxic therapy (NCT01740570 and NCT01866449). However, we propose that lower doses of these compounds could imitate the effect of TAU overexpression, reducing the aggressiveness of gliomas with less secondary effects for the patients. By contrast, as they compete for the same microtubule binding site of TAU, the presence of this protein could identify gliomas that would be resistant to taxol derivatives, as it has been shown for other cancers (*59*).

There are several limitations related to our study. The high intratumoral heterogeneity, with different tumor subtypes coexisting in different glioma regions (*60*), might complicate the outcome of a potential microtubule-stabilizer approach. Regarding the mechanism, we have shown that the increase in the methylation of the *MAPT* promoter is responsible for the induction of its expression. However, we cannot discard that hypermethylation of histones, which are responsible for some of the IDH mut phenotypes (*14*), could be modulating *MAPT* transcription as well. Moreover, we have described in detail the tumor suppressor functions of TAU in gliomas. Nonetheless, we could speculate that this protein might be participating in early steps of gliomagenesis or regulating other pro-oncogenic functions like cellular invasion or vascular co-option. Both of them have been associated with the expression of OLIG2 in gliomas (*61*, *62*). In any case, our results provide a possible explanation for the better outcome of IDH mut gliomas, which could have important implications for several aspects of glioma research and clinical practice. Moreover, understanding how TAU governs the vascular component of the TME in gliomas could provide insight for the neurovascular dysfunction observed in AD and other dementias.

MATERIALS AND METHODS

Study design

Our overall objective was to characterize the expression and function of TAU in gliomas. For that, we used publically available cohorts of

human gliomas and samples obtained in the participating hospitals. We performed most of the analysis of TAU overexpression or downregulation in different orthotopic mouse models, including xenografts of human primary cells and mouse glioma allografts. We also used subcutaneous xenografts to analyze the function of TAU in a limited dilution assay. Sample size for those animal experiments was determined before the study as per Institutional Research Ethics and Animal Welfare Committee (CEIyBA) guidelines. Experiments were designed to detect 20% differences between treatment groups or genotype-dependent effects at 80% power ($\alpha = 0.05$). The subjects were not randomly assigned to experimental groups because of animal housing considerations. Treatments were not administered blinded; however, mice were monitored for signs of distress and humane endpoints in a blinded manner. Regarding in vitro experiments, all the assays were performed with at least triplicate samples. No outliers were excluded. Where possible, studies have been repeated by independent personnel.

Human samples

Glioma tissues (fresh frozen or embedded in paraffin) were obtained after patient's written consent and with the approval of the Ethical Committees of "Hospital 12 de Octubre" (CEI 14/023) and "Hospitales de Madrid" (14.10.632-GHM, 18.12.1337-GHM) (tables S1 and S2).

Human and mouse glioma cells

RG1 cells were donated by R. Galli (San Raffaele Scientific Institute). The rest of the human cells (table S3) were obtained by dissociation of surgical specimens from patients treated at the Hospital 12 de Octubre (Madrid, Spain), after patient's written consent and with the approval of the Ethical Committee (CEI 14/023). They belong to the Biobank of that Hospital. Cells were grown in complete media (CM): Neurobasal supplemented with B27 (1:50) and GlutaMAX (1:100) (Thermo Fisher Scientific); penicillin-streptomycin (1:100) (Lonza); 0.4% heparin (Sigma-Aldrich); and EGF (40 ng/ml) and bFGF2 (20 ng/ml) (PeproTech). Mouse SVZ models were obtained by retroviral expression of EGFRwt or EGFRvIII in primary progenitors from p16/p19 ko mice. These cells were obtained as previously described (*63*), and they were grown in CM. After infection, the cells were injected into nude mice, and the tumors that grew were dissociated and established as SVZ-EGFRamp/wt or SVZ-EGFRvIII models. Both models express GFP and luciferase as reporters. These cell lines give rise to gliomas when they are implanted (300,000 cells) in the brains of nude mice with a 100% penetrance. The average survival is around 62 days for the SVZ-EGFRwt/amp and around 32 days for the SVZ-EGFRvIII cells, showing a proliferation rate of more than 10 and 30% in SVZ-EGFRwt/amp and SVZ-EGFRvIII tumors, respectively. Both mouse glioma models showed a complete dependence on EGFR activity because their growth can be impaired by a tyrosin kinase inhibitor (dacomitinib) (*44*). NPA (NRAS, shP53, and shATRX) IDH1 wt and NPA (NRAS, shP53, and shATRX) IDH1 R132H were provided by M. G. Castro (University of Michigan) (*14*) and cultured in CM.

Statistical analysis

For bar graphs, the significance was determined by a two-tailed unpaired Student's *t* test. The difference between experimental groups was assessed by paired *t* test and one-way analysis of variance (ANOVA). For Kaplan-Meier survival curves, the significance was determined by the two-tailed log-rank test. For correlation analysis between each gene, expression data were tested by Pearson's correlation coefficient and Spearman's correlation coefficient. All analyses were performed with the GraphPad Prism 5 software. *P* values <0.05 were considered significant ($*P < 0.05$; $**P < 0.01$; $***P < 0.001$; $****P < 0.0001$; n.s., not significant). All quantitative data presented are the means ± SEM from at least three samples or experiments per data point. Precise experimental details (number of animals or cells and experimental replicates) are provided in the figure legends.

SUPPLEMENTARY MATERIALS

stm.sciencemag.org/cgi/content/full/12/527/eaax1501/DC1

Materials and Methods

Fig. S1. Association of TAU with the clinical pathology of diffuse gliomas.

Fig. S2. Expression of TAU in PDX.

Fig. S3. TAU correlates with the presence of IDH mutations.

Fig. S4. The expression of *MAPT* is associated with the IDH mut DNA methylation phenotype.

Fig. S5. Association of TAU function with the EGFR pathway in gliomas.

Fig. S6. Association of TAU with the different GBM subtypes and the NF-κB–TAZ axis.

Fig. S7. Vascular phenotypes associated with TAZ in gliomas.

Fig. S8. Implication of the tumor-derived pericytes on the glioma vasculature and growth.

Fig. S9 TAU negatively correlates with EGFR signaling and *CD248* expression.

Fig. S10. The vascular phenotype of gliomas is determined by the genetic status of *EGFR* and *IDH* and by the expression of TAU.

Table S1. Human samples.

Table S2. Paired human samples.

Table S3. GBM cell lines.

Table S4. Antibodies.

Table S5. qRT-PCR primers.

Table S6. Sequencing primers.

Data file S1. Raw data.

View/request a protocol for this paper from *Bio-protocol*.

REFERENCES AND NOTES

1. D. N. Louis, A. Perry, G. Reifenberger, D. A. von, D. Figarella-Branger, W. K. Cavenee, H. Ohgaki, O. D. Wiestler, P. Kleihues, D. W. Ellison, The 2016 World Health Organization Classification of Tumors of the Central Nervous System: A summary. *Acta Neuropathol.* **131**, 803–820 (2016).
2. H. Yan, D. W. Parsons, G. Jin, R. M. Lendon, B. A. Rasheed, W. Yuan, I. Kos, I. Batinic-Haberle, S. Jones, G. J. Riggins, H. Friedman, A. Friedman, D. Reardon, J. Herndon, K. W. Kinzler, V. E. Velculescu, B. Vogelstein, D. D. Bigner, IDH1 and IDH2 mutations in gliomas. *N. Engl. J. Med.* **360**, 765–773 (2009).
3. S. Turcan, D. Rohle, A. Goenka, L. A. Walsh, F. Fang, E. Yilmaz, C. Campos, A. W. M. Fabius, C. Lu, P. S. Ward, C. B. Thompson, A. Kaufman, O. Guryanova, R. Levine, A. Heguy, A. Viale, L. G. T. Morris, J. T. Huse, I. K. Mellinghoff, T. A. Chan, IDH1 mutation is sufficient to establish the glioma hypermethylator phenotype. *Nature* **483**, 479–483 (2012).
4. C. Lu, P. S. Ward, G. S. Kapoor, D. Rohle, S. Turcan, O. Abdel-Wahab, C. R. Edwards, R. Khanin, M. E. Figueroa, A. Melnick, K. E. Wellen, D. M. O'Rourke, S. L. Berger, T. A. Chan, R. L. Levine, I. K. Mellinghoff, C. B. Thompson, IDH mutation impairs histone demethylation and results in a block to cell differentiation. *Nature* **483**, 474–478 (2012).
5. A. E. Calvert, A. Chalastanis, Y. Wu, L. A. Hurley, F. M. Kouri, Y. Bi, M. Kachman, J. L. May, E. Bartom, Y. Hua, R. K. Mishra, G. E. Schiltz, O. Dubrovskyi, A. P. Mazar, M. E. Peter, H. Zheng, C. D. James, C. F. Burant, N. S. Chandel, R. V. Davuluri, C. Horbinski, A. H. Stegh, Cancer-Associated IDH1 Promotes Growth and Resistance to Targeted Therapies in the Absence of Mutation. *Cell Rep.* **19**, 1858–1873 (2017).
6. R. J. Molenaar, J. P. Maciejewski, J. W. Wilmink, C. J. F. van Noorden, Wild-type and mutated IDH1/2 enzymes and therapy responses. *Oncogene* **37**, 1949–1960 (2018).
7. R. G. Verhaak, K. A. Hoadley, E. Purdom, V. Wang, Y. Qi, M. D. Wilkerson, C. R. Miller, L. Ding, T. Golub, J. P. Mesirov, G. Alexe, M. Lawrence, M. O'Kelly, P. Tamayo, B. A. Weir, S. Gabriel, W. Winckler, S. Gupta, L. Jakkula, H. S. Feiler, J. G. Hodgson, C. D. James, J. N. Sarkaria, C. Brennan, A. Kahn, P. T. Spellman, R. K. Wilson, T. P. Speed, J. W. Gray, M. Meyerson, G. Getz, C. M. Perou, D. N. Hayes; Cancer Genome Atlas Research Network, Integrated genomic analysis identifies clinically relevant subtypes of glioblastoma characterized by abnormalities in PDGFRA, IDH1, EGFR, and NF1. *Cancer Cell* **17**, 98–110 (2010).
8. K. Ichimura, Y. Narita, C. E. Hawkins, Diffusely infiltrating astrocytomas: pathology, molecular mechanisms and markers. *Acta Neuropathol.* **129**, 789–808 (2015).

9. J. Avila, E. G. de Barreda, A. Fuster-Matanzo, D. Simon, M. Llorens-Martin, T. Engel, J. J. Lucas, M. Diaz-Hernandez, F. Hernandez, Looking for novel functions of TAU. *Biochem. Soc. Trans.* **40**, 653–655 (2012).
10. E. G. Barreda, J. Avila, TAU regulates the subcellular localization of calmodulin. *Biochem. Biophys. Res. Commun.* **408**, 500–504 (2011).
11. H. Li, Z.-W. Duan, P. Xie, Y.-R. Liu, W.-C. Wang, S.-X. Dou, P.-Y. Wang, Effects of paclitaxel on EGFR endocytic trafficking revealed using quantum dot tracking in single cells. *PLOS ONE* **7**, e45465 (2012).
12. S. Lehrer, Glioblastoma and dementia may share a common cause. *Med. Hypotheses* **75**, 67–68 (2010).
13. R. Gargini, B. Segura-Collar, P. Sánchez-Gómez, Novel Functions of the Neurodegenerative-Related Gene TAU in Cancer. *Front. Aging Neurosci.* **11**, 231 (2019).
14. F. J. Núñez, F. M. Mendez, P. Kadiyala, M. S. Alghamri, M. G. Savelieff, M. B. Garcia-Fabiani, S. Haase, C. Koschmann, A.-A. Calinescu, N. Kamran, M. Saxena, R. Patel, S. Carney, M. Z. Guo, M. Edwards, M. Ljungman, T. Qin, M. A. Sartor, R. Tagett, S. Venneti, J. Brosnan-Cashman, A. Meeker, V. Gorbunova, L. Zhao, D. M. Kremer, L. Zhang, C. A. Lyssiotis, L. Jones, C. J. Herting, J. L. Ross, D. Hambardzumyan, S. Hervey-Jumper, M. E. Figueroa, P. R. Lowenstein, M. G. Castro, IDH1-R132H acts as a tumor suppressor in glioma via epigenetic up-regulation of the DNA damage response. *Sci. Transl. Med.* **11**, eaaq1427 (2019).
15. W. A. Flavahan, Y. Drier, B. B. Liau, S. M. Gillespie, A. S. Venteicher, A. O. Stemmer-Rachamimov, M. L. Suva, B. E. Bernstein, Insulator dysfunction and oncogene activation in IDH mutant gliomas. *Nature* **529**, 110–114 (2016).
16. M. L. Caillet-Boudin, L. Buee, N. Sergeant, B. Lefebvre, Regulation of human MAPT gene expression. *Mol. Neurodegener.* **10**, 28 (2015).
17. M. Perez, I. Santa-Maria, E. G. De Barreda, X. Zhu, R. Cuadros, J. R. Cabrero, F. Sanchez-Madrid, H. N. Dawson, M. P. Vitek, G. Perry, M. A. Smith, J. Avila, TAU-an inhibitor of deacetylase HDAC6 function. *J. Neurochem.* **109**, 1756–1766 (2009).
18. Y.-s. Gao, C. C. Hubbert, T.-P. Yao, The microtubule-associated histone deacetylase 6 (HDAC6) regulates epidermal growth factor receptor (EGFR) endocytic trafficking and degradation. *J. Biol. Chem.* **285**, 11219–11226 (2010).
19. B. Zhang, J. Carroll, J. Q. Trojanowski, Y. Yao, M. Iba, J. S. Potuzak, A.-M. L. Hogan, S. X. Xie, C. Ballatore, A. B. Smith III, V. M.-Y. Lee, K. R. Brunden, The microtubule-stabilizing agent, epothilone D, reduces axonal dysfunction, neurotoxicity, cognitive deficits, and Alzheimer-like pathology in an interventional study with aged TAU transgenic mice. *J. Neurosci.* **32**, 3601–3611 (2012).
20. K. P. L. Bhat, V. Balasubramaniyan, B. Vaillant, R. Ezhilarasan, K. Hummelink, F. Hollingsworth, K. Wani, L. Heathcock, J. D. James, L. D. Goodman, S. Conroy, L. Long, N. Lelic, S. Wang, J. Gumin, D. Raj, Y. Kodama, A. Raghunathan, A. Olar, K. Joshi, C. E. Pelloski, A. Heimberger, S. H. Kim, D. P. Cahill, G. Rao, W. F. A. Den Dunnen, H. W. G. M. Boddeke, H. S. Phillips, I. Nakano, F. F. Lang, H. Colman, E. P. Sulman, K. Aldape, Mesenchymal differentiation mediated by NF-κ B promotes radiation resistance in glioblastoma. *Cancer Cell* **24**, 331–346 (2013).
21. N. Pozo, C. Zahonero, P. Fernández, J. M. Liñares, A. Ayuso, M. Hagiwara, A. Pérez, J. R. Ricoy, A. Hernández-Laín, J. M. Sepúlveda, P. Sánchez-Gómez, Inhibition of DYRK1A destabilizes EGFR and reduces EGFR-dependent glioblastoma growth. *J. Clin. Invest.* **123**, 2475–2487 (2013).
22. F. Lu, Y. Chen, C. Zhao, H. Wang, D. He, L. Xu, J. Wang, X. He, Y. Deng, E. E. Lu, X. Liu, R. Verma, H. Bu, R. Drissi, M. Fouladi, A. O. Stemmer-Rachamimov, D. Burns, M. Xin, J. B. Rubin, E. M. Bahassi, P. Canoll, E. C. Holland, Q. R. Lu, Olig 2-Dependent Reciprocal Shift in PDGF and EGF Receptor Signaling Regulates Tumor Phenotype and Mitotic Growth in Malignant Glioma. *Cancer Cell* **29**, 669–683 (2016).
23. N. García-Romero, C. González-Tejedo, J. Carrión-Navarro, S. Esteban-Rubio, G. Rackov, V. Rodríguez-Fanjul, J. Oliver-De La Cruz, R. Prat-Acín, M. Peris-Celda, D. Blesa, L. Ramírez-Jiménez, P. Sánchez-Gómez, R. Perona, C. Escobedo-Lucea, C. Belda-Iniesta, A. Ayuso-Sacido, Cancer stem cells from human glioblastoma resemble but do not mimic original tumors after in vitro passaging in serum-free media. *Oncotarget* **7**, 65888–65901 (2016).
24. S. Bougnaud, A. Golebiewska, A. Oudin, O. Keunen, P. N. Harter, L. Mäder, F. Azuaje, S. Fritah, D. Stieber, T. Kaoma, L. Vallar, N. H. Brons, T. Daubon, H. Miletic, T. Sundstrøm, C. Herold-Mende, M. Mittelbronn, R. Bjerkvig, S. P. Niclou, Molecular crosstalk between tumour and brain parenchyma instructs histopathological features in glioblastoma. *Oncotarget* **7**, 31955–31971 (2016).
25. G. Bergers, S. Song, The role of pericytes in blood-vessel formation and maintenance. *Neuro-Oncology* **7**, 452–464 (2005).
26. S. Scully, R. Francescone, M. Faibish, B. Bentley, S. L. Taylor, D. Oh, R. Schapiro, L. Moral, W. Yan, R. Shao, Transdifferentiation of glioblastoma stem-like cells into mural cells drives vasculogenic mimicry in glioblastomas. *J. Neurosci.* **32**, 12950–12960 (2012).
27. L. Cheng, Z. Huang, W. Zhou, Q. Wu, S. Donnola, J. K. Liu, X. Fang, A. E. Sloan, Y. Mao, J. D. Lathia, W. Min, R. E. McLendon, J. N. Rich, S. Bao, Glioblastoma stem cells generate vascular pericytes to support vessel function and tumor growth. *Cell* **153**, 139–152 (2013).
28. W. Zhou, C. Chen, Y. Shi, Q. Wu, R. C. Gimple, X. Fang, Z. Huang, K. Zhai, S. Q. Ke, Y. F. Ping, H. Feng, J. N. Rich, J. S. Yu, S. Bao, X. W. Bian, Targeting Glioma Stem Cell-Derived Pericytes Disrupts the Blood-Tumor Barrier and Improves Chemotherapeutic Efficacy. *Cell Stem Cell* **21**, 591–603.e4 (2017).
29. M. E. Hardee, D. Zagzag, Mechanisms of glioma-associated neovascularization. *Am. J. Pathol.* **181**, 1126–1141 (2012).
30. J. S. Park, I. K. Kim, S. Han, I. Park, C. Kim, J. Bae, S. J. Oh, S. Lee, J. H. Kim, D. C. Woo, Y. He, H. G. Augustin, I. Kim, D. Lee, G. Y. Koh, Normalization of Tumor Vessels by Tie 2 Activation and Ang2 Inhibition Enhances Drug Delivery and Produces a Favorable Tumor Microenvironment. *Cancer Cell* **30**, 953–967 (2016).
31. N. Simonavicius, D. Robertson, D. A. Bax, C. Jones, I. J. Huijbers, C. M. Isacke, Endosialin (CD248) is a marker of tumor-associated pericytes in high-grade glioma. *Mod. Pathol.* **21**, 308–315 (2008).
32. J. C. Buckner, A. Chakravarti, W. J. Curran Jr., Radiation plus Chemotherapy in Low-Grade Glioma. *N. Engl. J. Med.* **375**, 490–491 (2016).
33. J. G. Cairncross, M. Wang, R. B. Jenkins, E. G. Shaw, C. Giannini, D. G. B. C. Buckner, K. L. Fink, L. Souhami, N. J. Laperriere, J. T. Huse, M. P. Mehta, W. J. Curran Jr., Benefit from procarbazine, lomustine, and vincristine in oligodendroglial tumors is associated with mutation of IDH. *J. Clin. Oncol.* **32**, 783–790 (2014).
34. N. M. Amankulor, Y. Kim, S. Arora, J. Kargl, F. Szulzewsky, M. Hanke, D. H. Margineantu, A. Rao, H. Bolouri, J. Delrow, D. Hockenbery, A. McGarry Houghton, E. C. Holland, Mutant IDH1 regulates the tumor-associated immune system in gliomas. *Genes Dev.* **31**, 774–786 (2017).
35. Y. Yao, A. K.-Y. Chan, Z. Y. Qin, L. C. Chen, X. Zhang, J. C.-S. Pang, H. M. Li, Y. Wang, Y. Mao, H.-K. Ng, L. F. Zhou, Mutation analysis of IDH1 in paired gliomas revealed IDH1 mutation was not associated with malignant progression but predicted longer survival. *PLOS ONE* **8**, e67421 (2013).
36. B. E. Johnson, T. Mazor, C. Hong, M. Barnes, K. Aihara, C. Y. McLean, S. D. Fouse, S. Yamamoto, H. Ueda, K. Tatsuno, S. Asthana, L. E. Jalbert, S. J. Nelson, A. W. Bollen, W. C. Gustafson, E. Charron, W. A. Weiss, I. V. Smirnov, J. S. Song, A. B. Olshen, S. Cha, Y. Zhao, R. A. Moore, A. J. Mungall, S. J. M. Jones, M. Hirst, M. A. Marra, N. Saito, H. Aburatani, A. Mukasa, M. S. Berger, S. M. Chang, B. S. Taylor, J. F. Costello, Mutational analysis reveals the origin and therapy-driven evolution of recurrent glioma. *Science* **343**, 189–193 (2014).
37. T. Watanabe, S. Nobusawa, P. Kleihues, H. Ohgaki, IDH1 mutations are early events in the development of astrocytomas and oligodendrogliomas. *Am. J. Pathol.* **174**, 1149–1153 (2009).
38. C. Bardella, O. Al-Dalahmah, D. Krell, P. Brazauskas, K. Al-Qahtani, M. Tomkova, J. Adam, S. Serres, H. Lockstone, L. Freeman-Mills, I. Pfeffer, N. Sibson, R. Goldin, B. Schuster-Böeckler, P. J. Pollard, T. Soga, J. S. McCullagh, C. J. Schofield, P. Mulholland, O. Ansorge, S. Kriaucionis, P. J. Ratcliffe, F. G. Szele, I. Tomlinson, Expression of Idh1(R132H) in the Murine Subventricular Zone Stem Cell Niche Recapitulates Features of Early Gliomagenesis. *Cancer Cell* **30**, 578–594 (2016).
39. B. Philip, D. X. Yu, M. R. Silvis, C. H. Shin, J. P. Robinson, G. L. Robinson, A. E. Welker, S. N. Angel, S. R. Tripp, J. A. Sonnen, M. W. VanBrocklin, R. J. Gibbons, R. E. Looper, H. Colman, S. L. Holmen, Mutant IDH1 Promotes Glioma Formation In Vivo. *Cell Rep.* **23**, 1553–1564 (2018).
40. D. Rohle, J. Popovici-Muller, N. Palaskas, S. Turcan, C. Grommes, C. Campos, J. Tsoi, O. Clark, B. Oldrini, E. Komisopoulou, K. Kunii, A. Pedraza, S. Schalm, L. Silverman, A. Miller, F. Wang, H. Yang, Y. Chen, A. Kernytsky, M. K. Rosenblum, W. Liu, S. A. Biller, S. M. Su, C. W. Brennan, T. A. Chan, T. G. Graeber, K. E. Yen, I. K. Mellinghoff, An inhibitor of mutant IDH1 delays growth and promotes differentiation of glioma cells. *Science* **340**, 626–630 (2013).
41. D. Golub, N. Iyengar, S. Dogra, T. Wong, D. Bready, K. Tang, A. S. Modrek, D. G. Placantonakis, Mutant isocitrate dehydrogenase inhibitors as targeted cancer therapeutics. *Front. Oncol.* **9**, 417 (2019).
42. R. J. Molenaar, D. Botman, M. A. Smits, V. V. Hira, S. A. van Lith, J. Stap, P. Henneman, M. Khurshed, K. Lenting, A. N. Mul, D. Dimitrakopoulou, C. M. van Drunen, R. A. Hoebe, T. Radivoyevitch, J. W. Wilmink, J. P. Maciejewski, W. P. Vandertop, W. P. Leenders, F. E. Bleeker, C. J. van Noorden, Radioprotection of IDH1-Mutated Cancer Cells by the IDH1-Mutant Inhibitor AGI-5198. *Cancer Res.* **75**, 4790–4802 (2015).
43. M. Khurshed, N. Aarnoudse, R. Hulsbos, V. V. V. Hira, H. W. M. van Laarhoven, J. W. Wilmink, R. J. Molenaar, C. J. F. van Noorden, IDH1-mutant cancer cells are sensitive to cisplatin and an IDH1-mutant inhibitor counteracts this sensitivity. *FASEB J.* **32**, 6344–6352 (2018).
44. X. Wu, L. Sooman, J. Lennartsson, S. Bergstrom, M. Bergqvist, J. Gullbo, S. Ekman, Microtubule inhibition causes epidermal growth factor receptor inactivation in oesophageal cancer cells. *Int. J. Oncol.* **42**, 297–304 (2013).
45. C. Zahonero, P. Sanchez-Gomez, EGFR-dependent mechanisms in glioblastoma: Towards a better therapeutic strategy. *Cell. Mol. Life Sci.* **71**, 3465–3488 (2014).
46. M. V. Grandal, R. Zandi, M. W. Pedersen, B. M. Willumsen, B. van Deurs, H. S. Poulsen, EGFRvIII escapes down-regulation due to impaired internalization and sorting to lysosomes. *Carcinogenesis* **28**, 1408–1417 (2007).

47. R. Bonavia, M. M. Inda, S. Vandenberg, S. Y. Cheng, M. Nagane, P. Hadwiger, P. Tan, D. W. Sah, W. K. Cavenee, F. B. Furnari, EGFRvIII promotes glioma angiogenesis and growth through the NF-kappa B, interleukin-8 pathway. *Oncogene* **31**, 4054–4066 (2012).
48. R. Gargini, M. Escoll, E. Garcia, R. Garcia-Escudero, F. Wandosell, I. M. Anton, WIP Drives Tumor Progression through YAP/TAZ-Dependent Autonomous Cell Growth. *Cell Rep.* **17**, 1962–1977 (2016).
49. M. Ferraiuolo, C. Pulito, M. Finch-Edmondson, E. Korita, A. Maidecchi, S. Donzelli, P. Muti, M. Serra, M. Sudol, S. Strano, G. Blandino, Agave negatively regulates YAP and TAZ transcriptionally and post-translationally in osteosarcoma cell lines. *Cancer Lett.* **433**, 18–32 (2018).
50. A. Lai, S. Kharbanda, W. B. Pope, A. Tran, O. E. Solis, F. Peale, W. F. Forrest, K. Pujara, J. A. Carrillo, A. Pandita, B. M. Ellingson, C. W. Bowers, R. H. Soriano, N. O. Schmidt, S. Mohan, W. H. Yong, S. Seshagiri, Z. Modrusan, Z. Jiang, K. D. Aldape, P. S. Mischel, L. M. Liau, C. J. Escovedo, W. Chen, P. L. Nghiemphu, C. D. James, M. D. Prados, M. Westphal, K. Lamszus, T. Cloughesy, H. S. Phillips, Evidence for sequenced molecular evolution of IDH1 mutant glioblastoma from a distinct cell of origin. *J. Clin. Oncol.* **29**, 4482–4490 (2011).
51. D. Unruh, S. R. Schwarze, L. Khoury, C. Thomas, M. Wu, L. Chen, R. Chen, Y. Liu, M. A. Schwartz, C. Amidei, P. Kumthekar, C. G. Benjamin, K. Song, C. Dawson, J. M. Rispoli, G. Fatterpekar, J. G. Golfinos, D. Kondziolka, M. Karajannis, D. Pacione, D. Zagzag, T. M. Intyre, M. Snuderl, C. Horbinski, Mutant IDH1 and thrombosis in gliomas. *Acta Neuropathol.* **132**, 917–930 (2016).
52. P. Kickingereder, F. Sahm, A. Radbruch, W. Wick, S. Heiland, A. Deimling, M. Bendszus, B. Wiestler, IDH mutation status is associated with a distinct hypoxia/angiogenesis transcriptome signature which is non-invasively predictable with rCBV imaging in human glioma. *Sci. Rep.* **5**, 16238 (2015).
53. R. Missiaen, M. Mazzone, G. Bergers, The reciprocal function and regulation of tumor vessels and immune cells offers new therapeutic opportunities in cancer. *Semin. Cancer Biol.* **52**, 107–116 (2018).
54. N. Pallas-Bazarra, J. Jurado-Arjona, M. Navarrete, J. A. Esteban, F. Hernández, J. Ávila, M. Llorens-Martin, Novel function of TAU in regulating the effects of external stimuli on adult hippocampal neurogenesis. *EMBO J.* **35**, 1417–1436 (2016).
55. A. A. Podtelezhnikov, K. Q. Tanis, M. Nebozhyn, W. J. Ray, D. J. Stone, A. P. Loboda, Molecular insights into the pathogenesis of Alzheimer's disease and its relationship to normal aging. *PLOS ONE* **6**, e29610 (2011).
56. K. Kisler, A. R. Nelson, A. Montagne, B. V. Zlokovic, Cerebral blood flow regulation and neurovascular dysfunction in Alzheimer disease. *Nat. Rev. Neurosci.* **18**, 419–434 (2017).
57. A. P. Sagare, R. D. Bell, Z. Zhao, Q. Ma, E. A. Winkler, A. Ramanathan, B. V. Zlokovic, Pericyte loss influences Alzheimer-like neurodegeneration in mice. *Nat. Commun.* **4**, 2932 (2013).
58. D. Semiond, S. S. Sidhu, M. C. Bissery, P. Vrignaud, Can taxanes provide benefit in patients with CNS tumors and in pediatric patients with tumors? An update on the preclinical development of cabazitaxel. *Cancer Chemother. Pharmacol.* **72**, 515–528 (2013).
59. M. Smoter, L. Bodnar, R. Duchnowska, R. Stec, B. Grala, C. Szczylik, The role of TAU protein in resistance to paclitaxel. *Cancer Chemother. Pharmacol.* **68**, 553–557 (2011).
60. A. Sottoriva, I. Spiteri, S. G. Piccirillo, A. Touloumis, V. P. Collins, J. C. Marioni, C. Curtis, C. Watts, S. Tavaré, Intratumor heterogeneity in human glioblastoma reflects cancer evolutionary dynamics. *Proc. Natl. Acad. Sci. U.S.A.* **110**, 4009–4014 (2013).
61. I. Nevo, K. Woolard, M. Cam, A. Li, J. D. Webster, Y. Kotliarov, H. S. Kim, S. Ahn, J. Walling, S. Kotliarova, G. Belova, H. Song, R. Bailey, W. Zhang, H. A. Fine, Identification of molecular pathways facilitating glioma cell invasion in situ. *PLOS ONE* **9**, e111783 (2014).
62. A. Griveau, G. Seano, S. J. Shelton, R. Kupp, A. Jahangiri, K. Obernier, S. Krishnan, O. R. Lindberg, T. J. Yuen, A. C. Tien, J. K. Sabo, N. Wang, I. Chen, J. Kloepper, L. Larrouquere, M. Ghosh, I. Tirosh, E. Huillard, A. Alvarez-Buylla, M. C. Oldham, A. I. Persson, W. A. Weiss, T. T. Batchelor, A. Stemmer-Rachamimov, M. L. Suvà, J. J. Phillips, M. K. Aghi, S. Mehta, R. K. Jain, D. H. Rowitch, A Glial Signature and Wnt 7 Signaling Regulate Glioma-Vascular Interactions and Tumor Microenvironment. *Cancer Cell* **33**, 874–889.e7 (2018).
63. S. R. Ferrón, C. Andreu-Agulló, H. Mira, P. Sánchez, M. Á. Marques-Torrejón, I. Fariñas, A combined ex/in vivo assay to detect effects of exogenously added factors in neural stem cells. *Nat. Protoc.* **2**, 849–859 (2007).

Acknowledgments: We acknowledge R. Galli for donating RG1, and R. Hortigüela and the confocal service personnel for technical support. The graphical abstract was created with images adapted from Servier Medical Art by Servier. **Funding:** This work was supported by NIH/NINDS grants R01-NS105556 and R37-ND094804 to M.G.C.; by Ministerio de Economía y Competitividad (Acción Estratégica en Salud) grants PI13/01258 to A.H.-L., PI17/01489 and CP11/00147 to A.A.-S., PI18/00263 to R.G.-E., and PI16/01 278 to J.S.; by "Asociación Española contra el Cancer" grants Investigador Junior to R.G. and GCTRA16015SEDA to J.M.S.-S. and J.S.; and by Ministerio de Economía y Competitividad SAF-2014-53040-P to J.A., RTC-2015-3771-1 to J.S., and SAF2015-65175-R/FEDER to P.S.-G. **Author contributions:** Conceptualization: R.G., B.S.-C., J.A., and P.S.-G. Development and characterization of mouse models: B.S.-C., R.G., and F.J.N. Resources (plasmids, mice, and human samples): V.G.-E., J.M.S.-S., A.P.-N., A.A.-S., J.S., and M.G.C. In vivo and in vitro experiments: R.G. and B.S.-C. In silico studies: R.G. and R.G.-E. mRNA and protein analysis: D.G.-P., A.R.-B., R.G., and B.S.-C. Histological analysis: A.H.-L., B.H., J.G.-G., R.G., and B.S.-C. Writing (original draft): R.G., B.S.-C., J.A., and P.S.-G. Writing (review and editing): V.G.-E., A.A.-S., J.S., J.M.S.-S., A.H.-L., M.G.C., and R.G.-E. Funding acquisition: R.G., J.A., and P.S.-G. Supervision: J.A. and P.S.-G. **Competing interests:** J.S. is the cofounder of Mosaic Biomedicals and a board member of Northern Biologics. J.M.S.-S. is a consultant for GW Pharma. J.S. received grant/research support from Mosaic Biomedicals, Northern Biologics, and Roche/Glycart. J.M.S.-S. received from Pfizer, and P.S.-G. from Servier, Catalysis, and IDP-Pharma. The rest of the authors declare that they have no competing interests. **Data and materials availability:** All data associated with this study are present in the paper or the Supplementary Materials.

Submitted 26 February 2019
Resubmitted 6 September 2019
Accepted 27 November 2019
Published 22 January 2020
10.1126/scitranslmed.aax1501

Citation: R. Gargini, B. Segura-Collar, B. Herránz, V. García-Escudero, A. Romero-Bravo, F. J. Núñez, D. García-Pérez, J. Gutiérrez-Guamán, A. Ayuso-Sacido, J. Seoane, A. Pérez-Núñez, J. M. Sepúlveda-Sánchez, A. Hernández-Laín, M. G. Castro, R. García-Escudero, J. Ávila, P. Sánchez-Gómez, The IDH-TAU-EGFR triad defines the neovascular landscape of diffuse gliomas. *Sci. Transl. Med.* **12**, eaax1501 (2020).

Science Translational Medicine

The IDH-TAU-EGFR triad defines the neovascular landscape of diffuse gliomas

Ricardo Gargini, Berta Segura-Collar, Beatriz Herránz, Vega García-Escudero, Andrés Romero-Bravo, Felipe J. Núñez, Daniel García-Pérez, Jacqueline Gutiérrez-Guamán, Angel Ayuso-Sacido, Joan Seoane, Angel Pérez-Núñez, Juan M. Sepúlveda-Sánchez, Aurelio Hernández-Laín, María G. Castro, Ramón García-Escudero, Jesús Ávila and Pilar Sánchez-Gómez

Sci Transl Med **12**, eaax1501.
DOI: 10.1126/scitranslmed.aax1501

The positive side of TAU

Gliomas, brain tumors originating in glial cells, are classified according to histologic as well as genetic features. Mutations in the IDH1/2 genes are associated with more favorable prognosis, whereas mutations in EGFR are characteristic of aggressive tumors. How these genes affect the microenvironment is not completely clear. Now, Gargini *et al.* show that TAU protein, classically associated with neurodegenerative disorders, is increased in less aggressive tumors. TAU inhibited the transition toward an aggressive phenotype by blocking EGFR activation. Mutated EGFR was no longer sensitive to TAU inhibition, possibly explaining the aggressive phenotype associated with EGFR mutations. The results suggest that TAU might play a main role in determining glioma aggressiveness.

Science Translational Medicine (ISSN 1946-6242) is published by the American Association for the Advancement of Science, 1200 New York Avenue NW, Washington, DC 20005. The title *Science Translational Medicine* is a registered trademark of AAAS.